LLNL-PRES-440231

Accretion Processes in Magnetic Cataclysmic Variables

Christopher Mauche

Physical and Life Sciences

Lawrence Livermore National Laboratory

This work was performed under the auspices of the U.S. Department of Energy by Lawrence Livermore National Security, LLC, Lawrence Livermore National Laboratory under Contract DE-AC52-07NA27344.

Introduction

I give a presentation based largely on X-ray grating spectroscopic observations of magnetic cataclysmic variables (CVs), interacting binaries in which the accretion flow is controlled by the ~ 0.1–100 MG magnetic field of the white dwarf.

I concentrate on:

- Physics aspects that are characteristic of these systems, such as high plasma densities and the effects of photoexcitation, photoionization, and fluorescence of the white dwarf surface and other plasma in the system.
- The relatively few systems for which we have good data (e.g., AM Her, EX Hya, AE Aqr).

The talk will include a minimal number of:

- light curves
- log-log plots
- broad-band spectral fits (no “mo wa po”).

Magnetic CVs come in two “flavors,” polars and intermediate polars

Polars

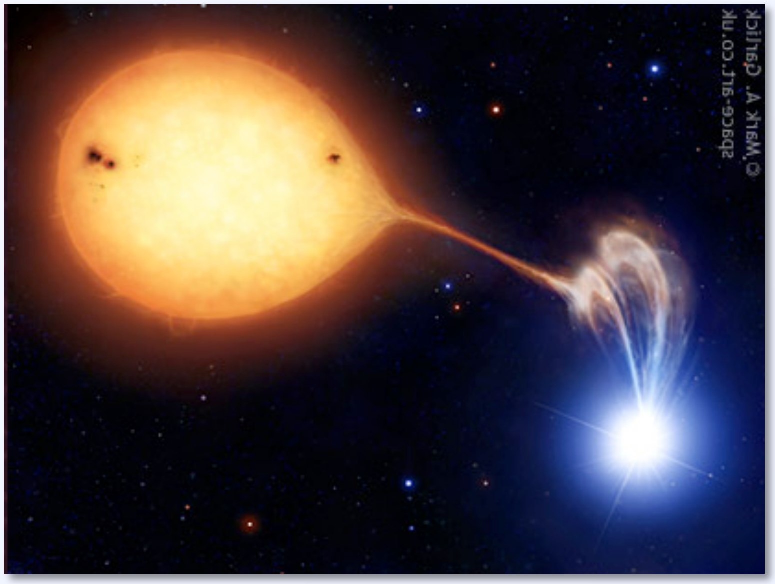

$B \sim$ 10–100 MG
No accretion disk
Synchronous rotation

Intermediate Polars

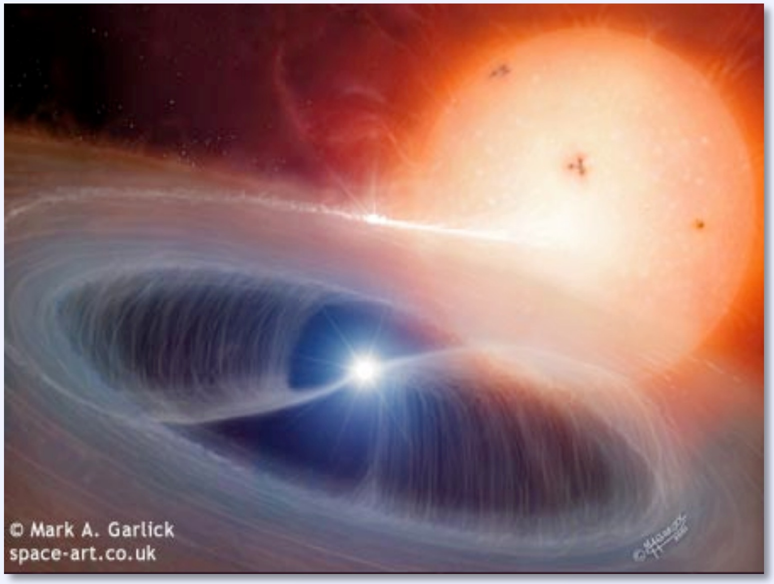

$B \sim$ 0.1–1 MG
Truncated accretion disk
Asynchronous rotation

Figures © Mark A. Garlick

In either case, X-rays are produced at and below the accretion shock

$kT_{shock} = \frac{3}{8} \mu m_H G M_{wd} / R_{wd}$

~ tens of keV

$kT_{bb} = (L_X / 4\pi\sigma f R_{wd}^2)^{1/4}$

~ tens of eV

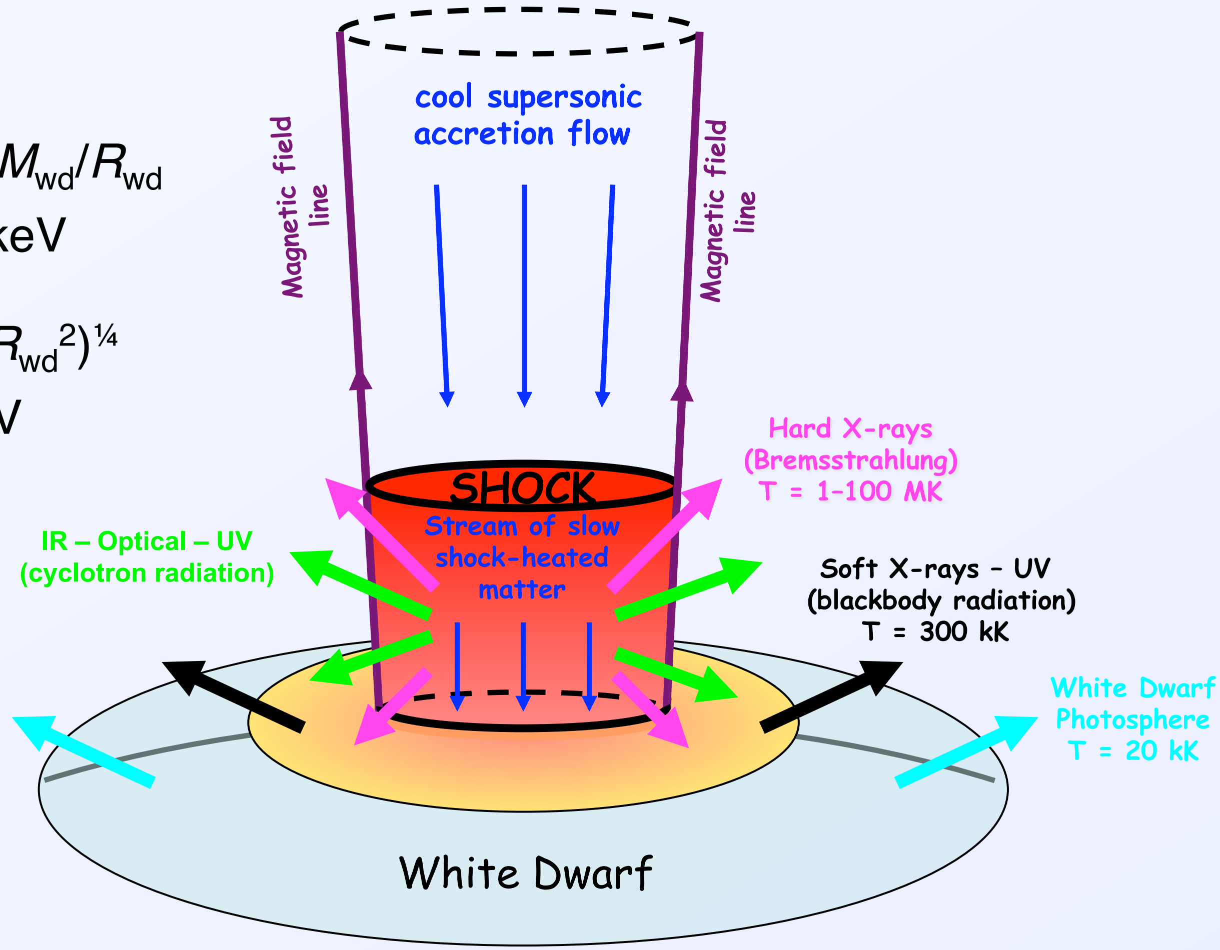

Figure courtesy of Vadim Burwitz

Example: *HEAO-1* A2 & A4 spectra of AM Her

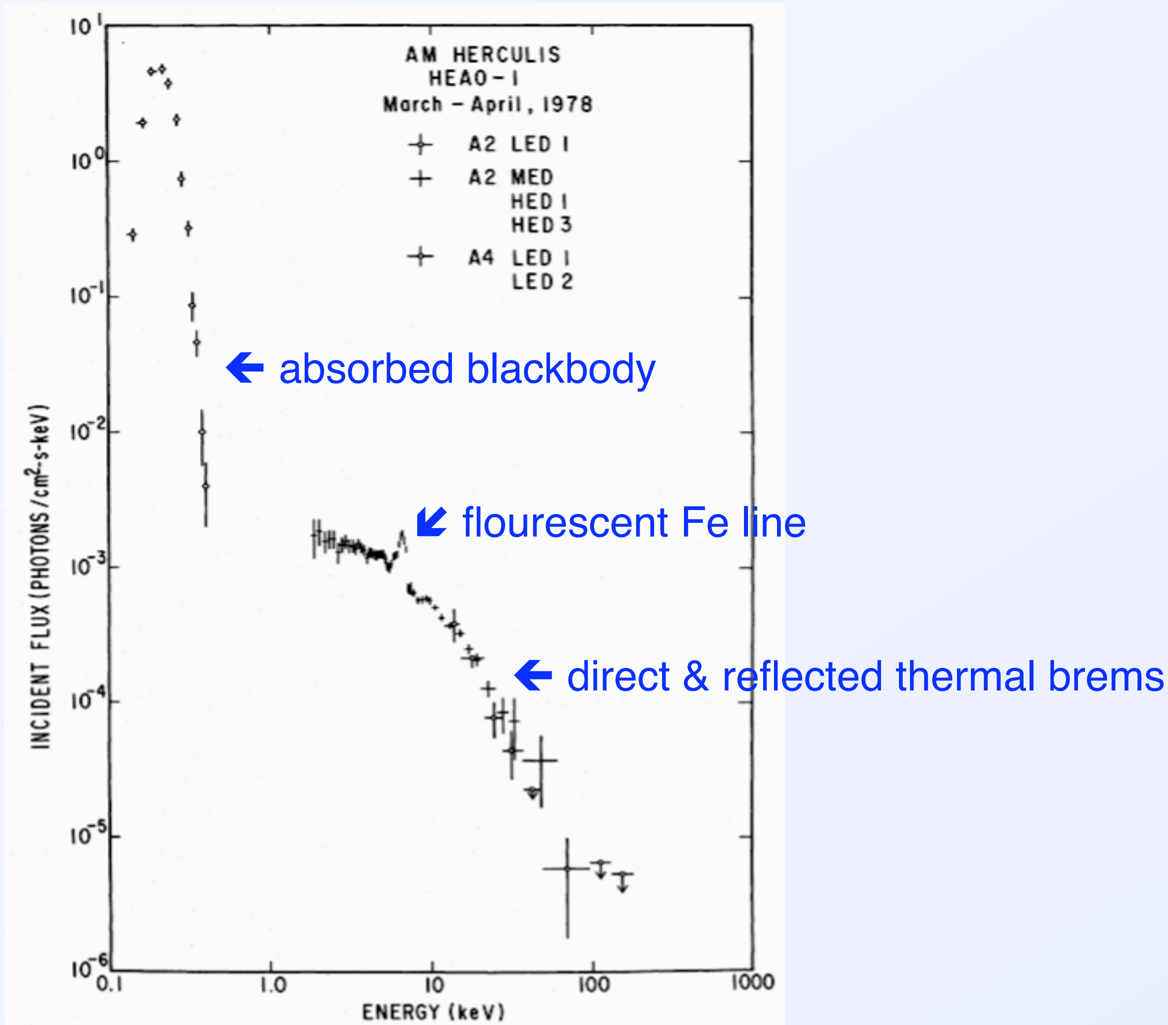

Rothschild et al. (1981, ApJ, 250,723)

EUVE SW spectra of VV Pup, AM Her, & QS Tel (RE 1838–461)

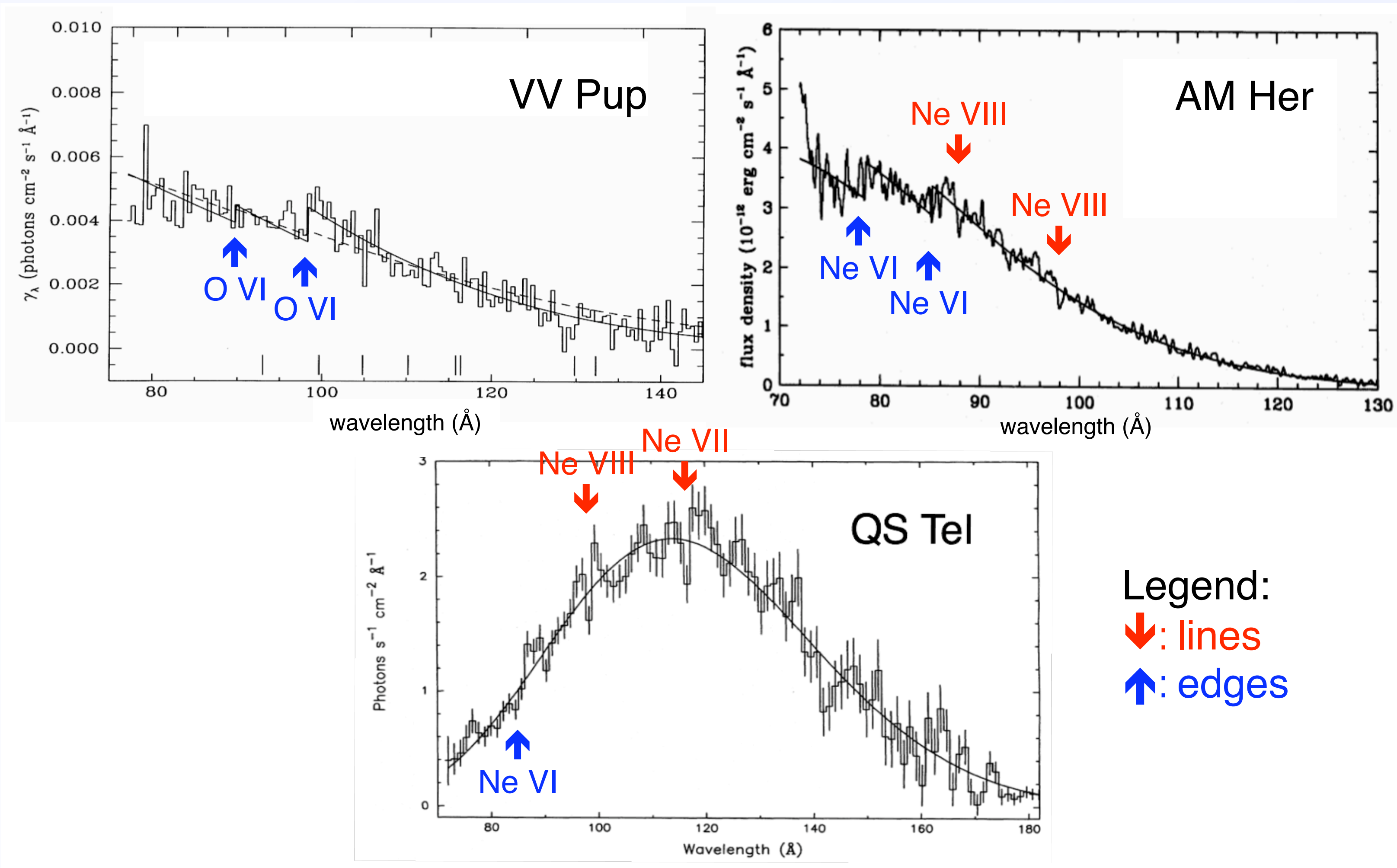

Vennes et al. (1995), Paerels et al. (1996), Rosen et al. (1996)

EUVE SW spectrum of AM Her

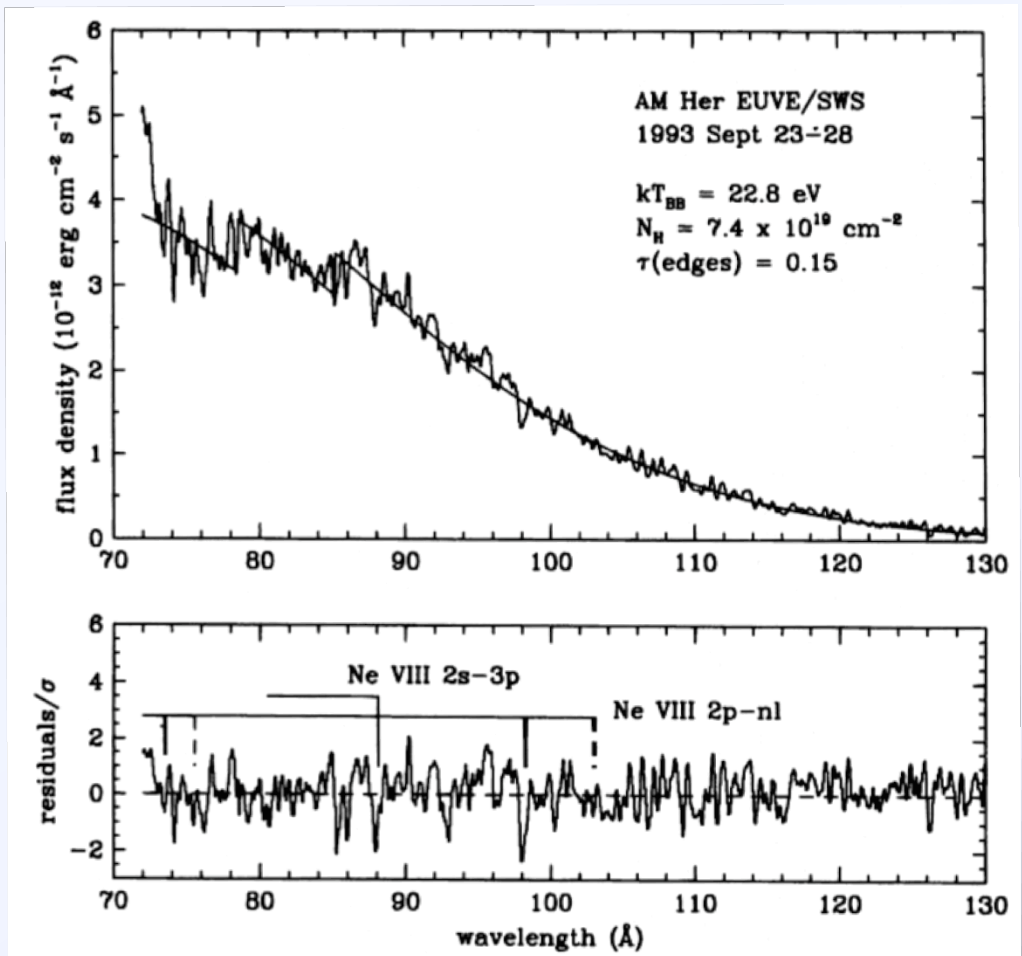

kT_{bb} = 22.8 eV
N_H = 7.4E19 cm^{-2}

Absorption edges:

- Ne VI $2s^2 2p$ λ78.5
- Ne VI $2s2p^2$ λ85.1

Discrete absorption features:

- Ne VIII 2s-3p λ88.1
- Ne VIII 2p-3d λ98.2

BUT: The observation was not "dithered" and **other than the 98.2 Å line**, these features have not been seen in subsequent observations.

Paerels, Hur, Mauche, & Heise (1996, ApJ, 464, 884)

EUVE SW spectra of nine polars

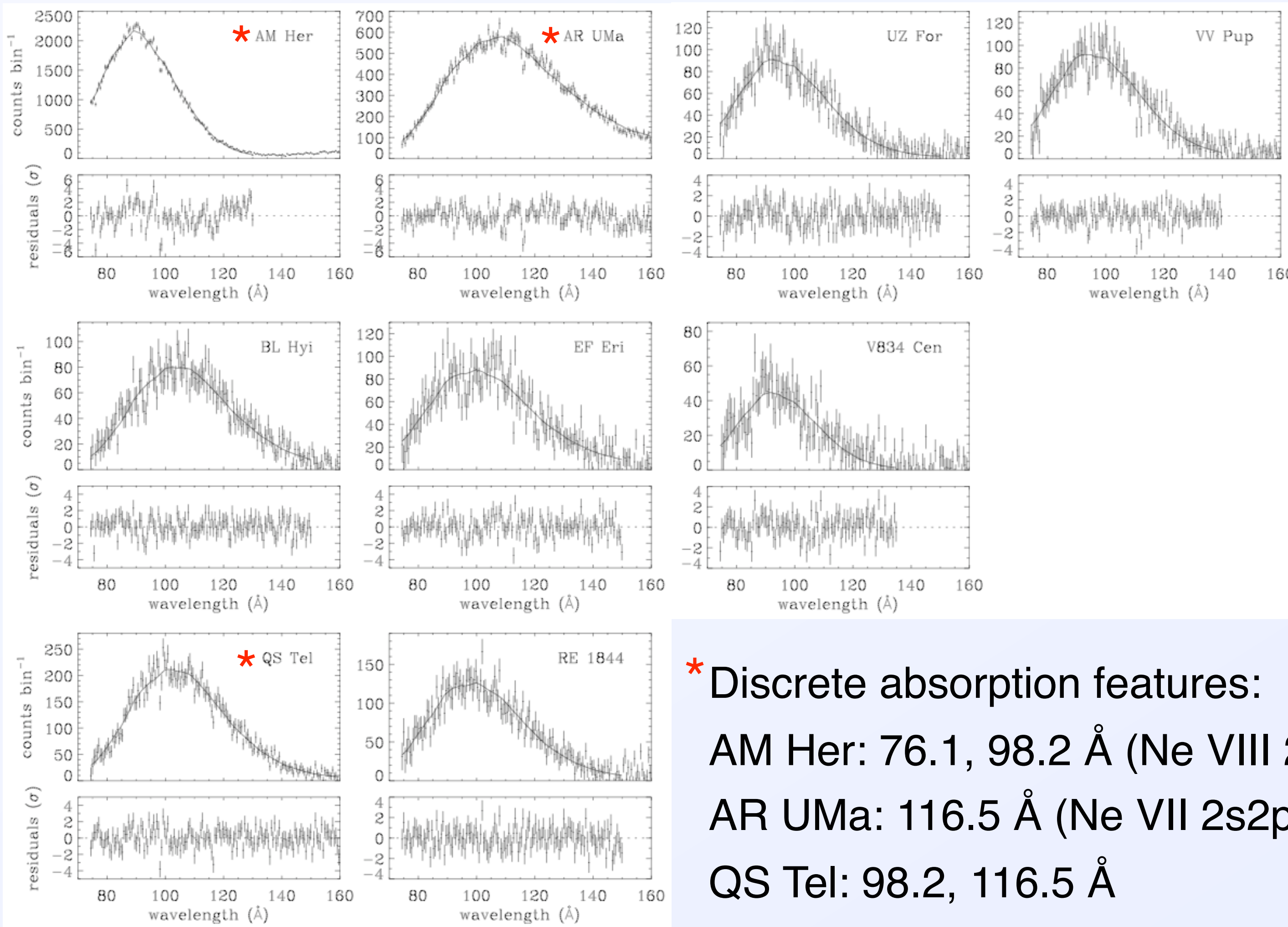

*Discrete absorption features:

AM Her: 76.1, 98.2 Å (Ne VIII 2p-3d)

AR UMa: 116.5 Å (Ne VII 2s2p-2s3d)

QS Tel: 98.2, 116.5 Å

Mauche (1999, in Annapolis Workshop on Magnetic CVs)

EUVE SW spectra of nine polars

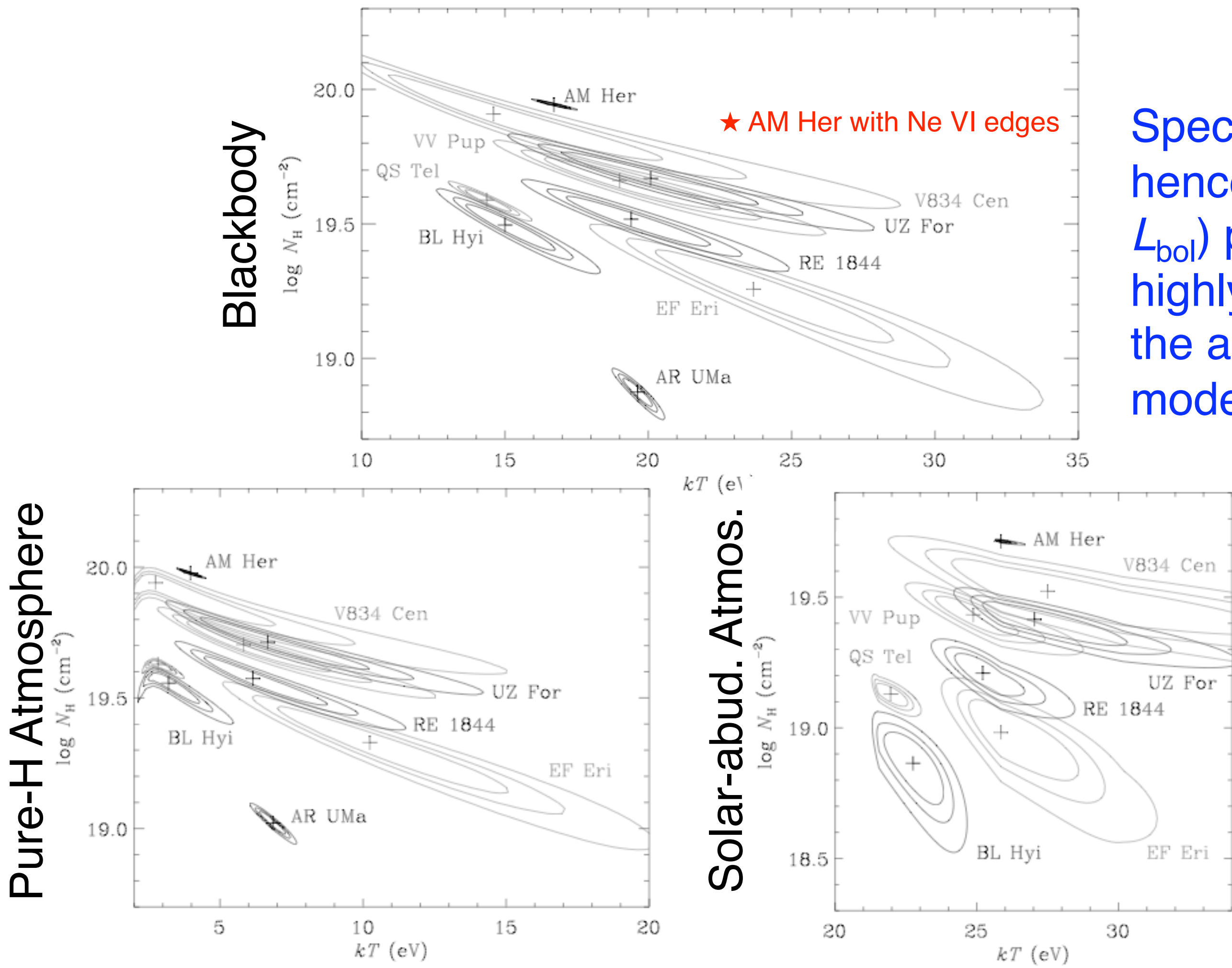

Spectral (kT, N_H) and hence physical (A_{spot}, L_{bol}) parameters are highly dependent on the assumed spectral model.

Mauche (1999, in Annapolis Workshop on Magnetic CVs)

Chandra LETG spectrum of AM Her

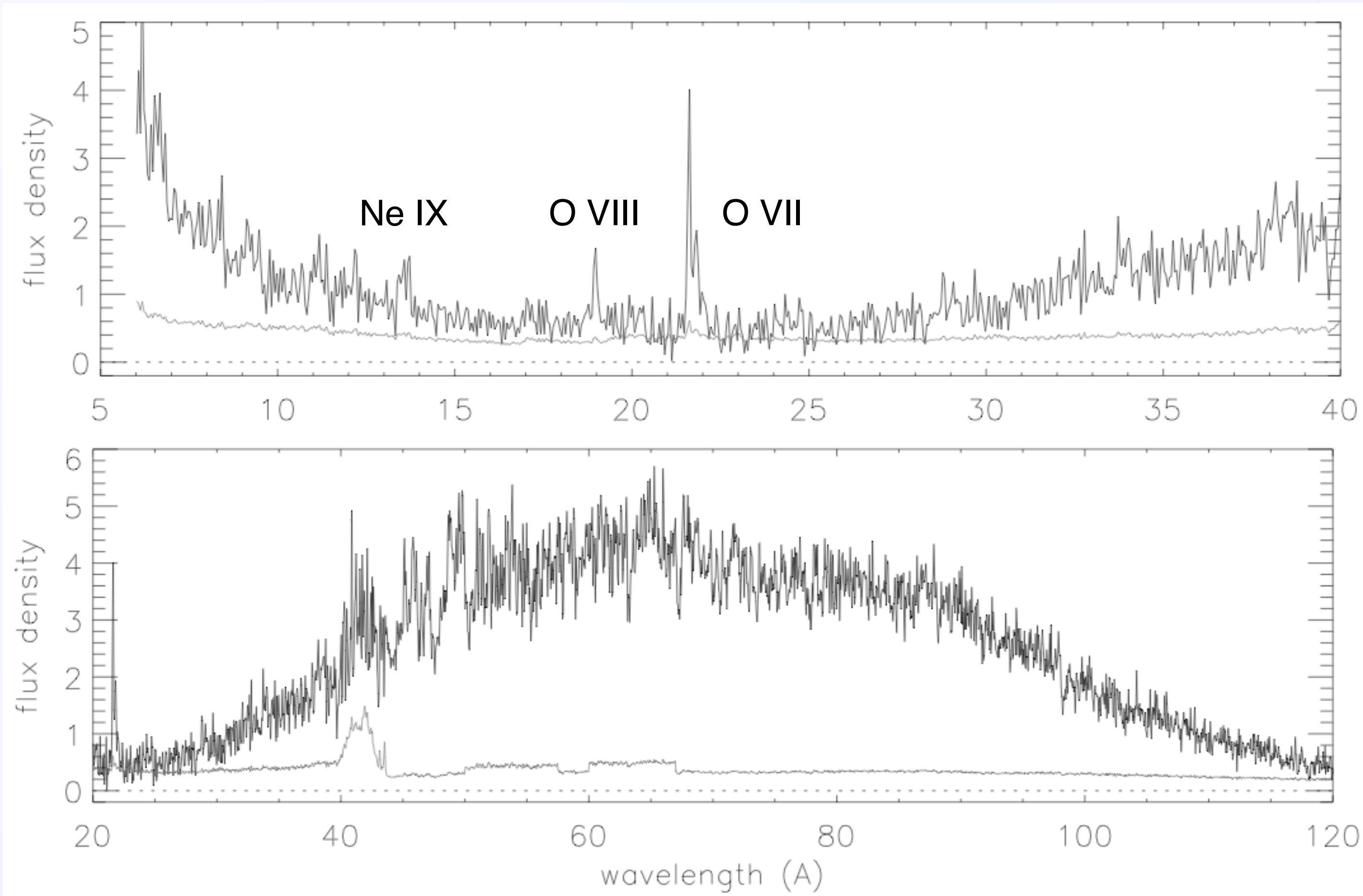

See also Burwitz et al. (2002, ASPC, 261, 137); Burwitz (2006, in High Resolution X-ray Spectroscopy: Towards *XEUS* and *Con-X*)

Chandra LETG spectrum of AM Her in and out of eclipse

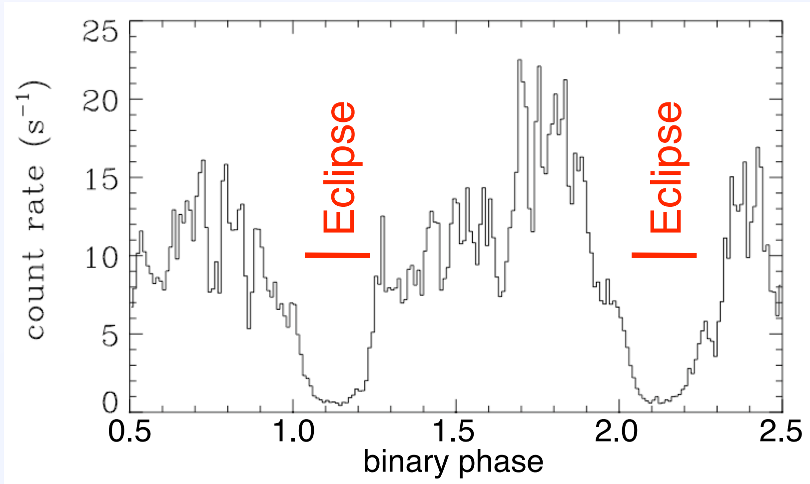

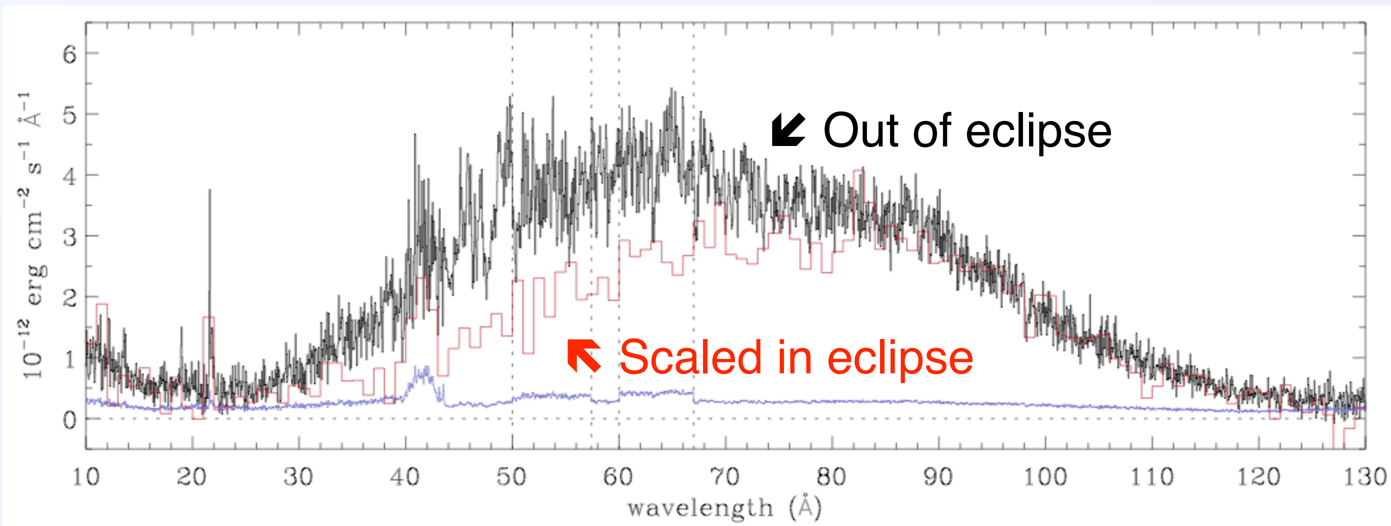

Phase-dependent spectrum implies a structured emission region.

Two types of X-ray spectra in CVs

Cooling Flow[1]: Non-magnetic*

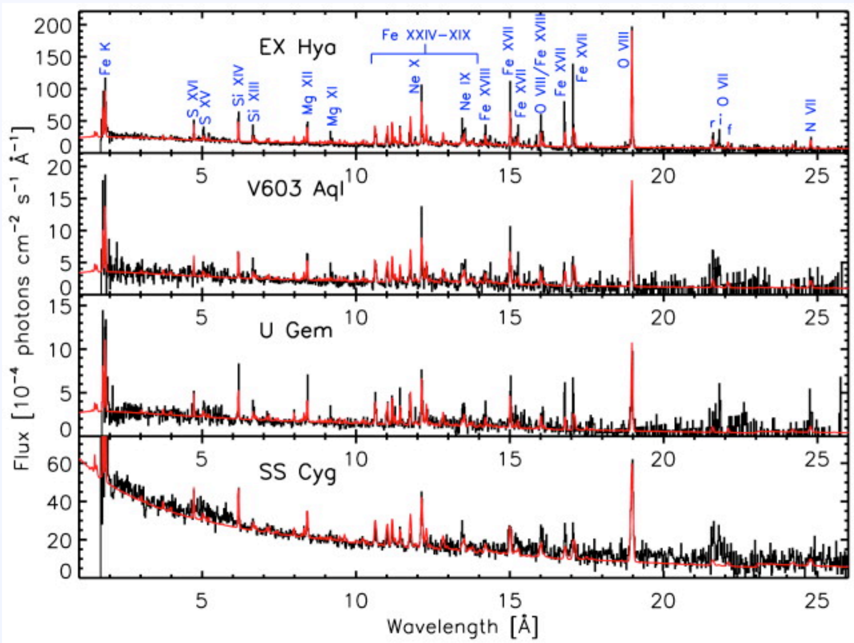

Photoionized[2]: Magnetic

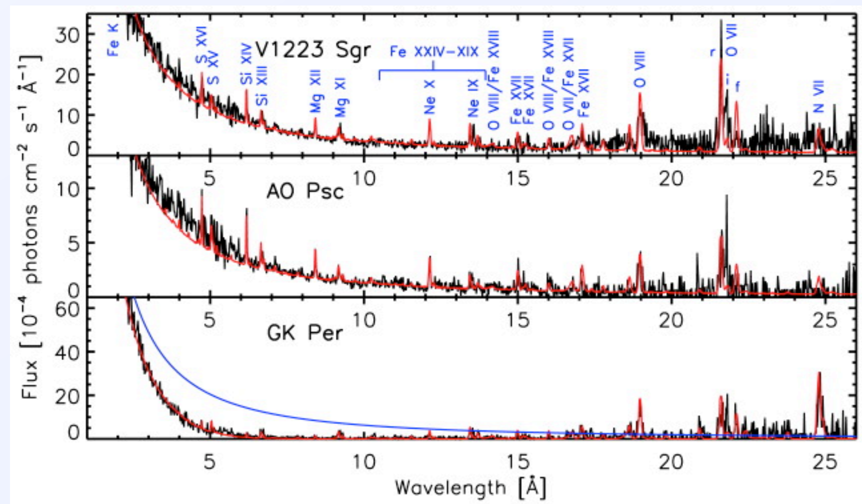

[1]Steady-state isobaric radiative cooling.

[2]Strong H- and He-like ion emission but weak Fe L-shell emission.

*With one exception: EX Hya [however, see Luna et al. (2010) {next slide}].

Mukai et al. (2003, ApJ, 586, 77)

EX Hya has weak broad photoionization emission features

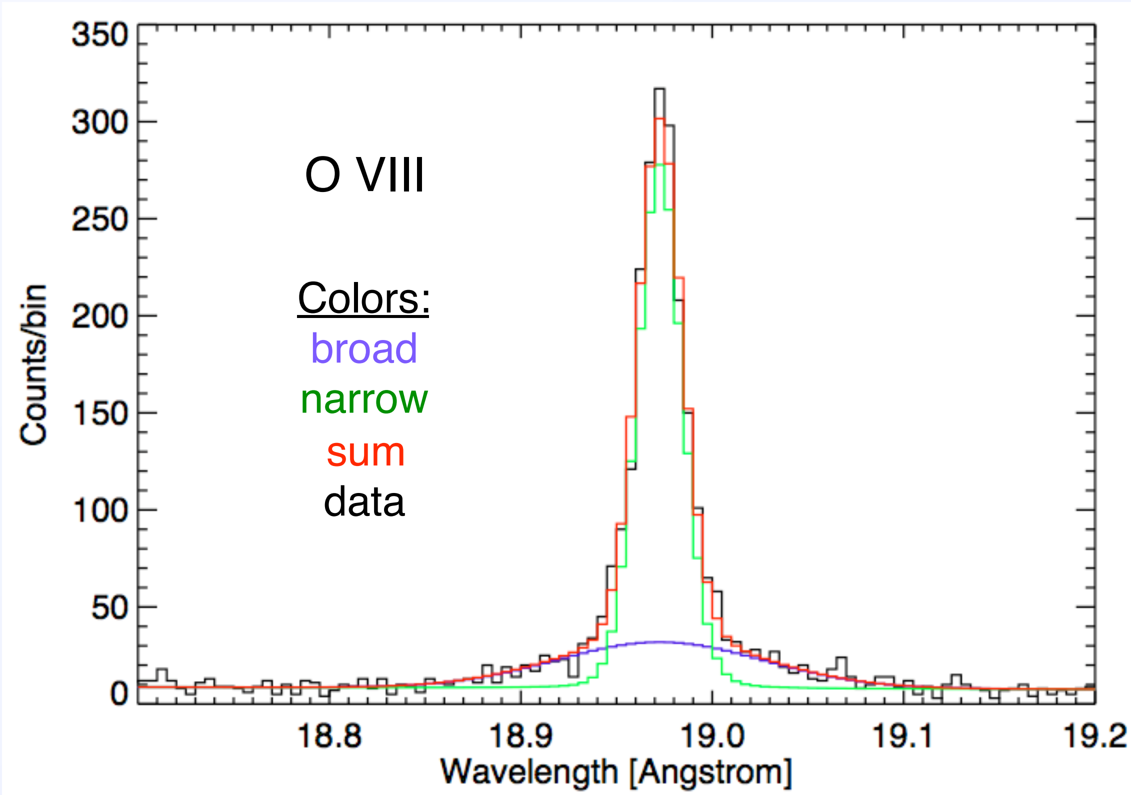

Broad component is formed in the pre-shock accretion flow, photoionized by radiation from the post-shock flow.

Luna et al. (2010, ApJ, 711, 1333)

Chandra HETG spectra of non-magnetic and magnetic CVs

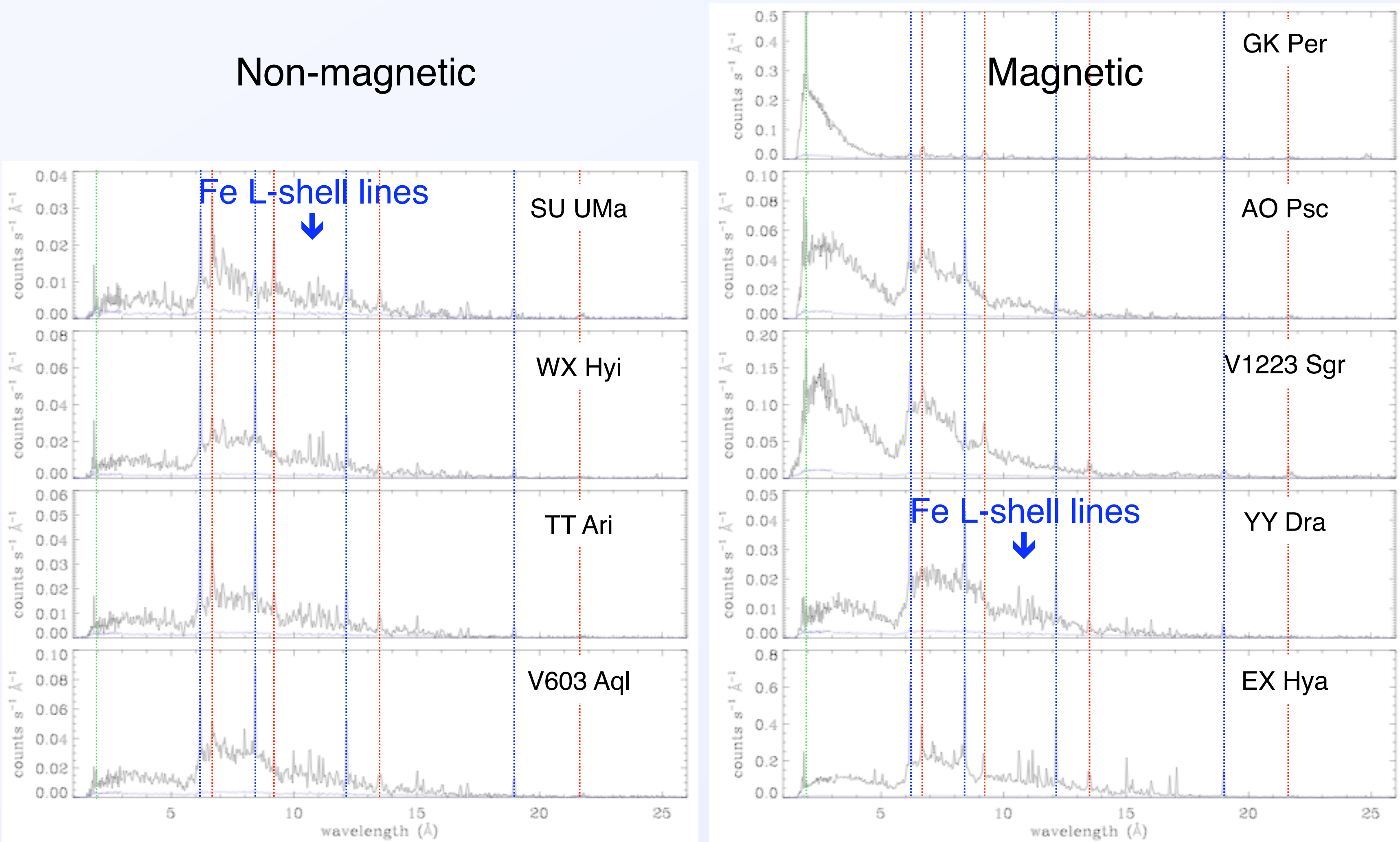

Division into two classes is no longer so clear-cut (see also Mukai 2009).

Contrary to indications from *ASCA* SIS spectra, the Fe K lines of magnetic CVs are not significantly Compton broadened

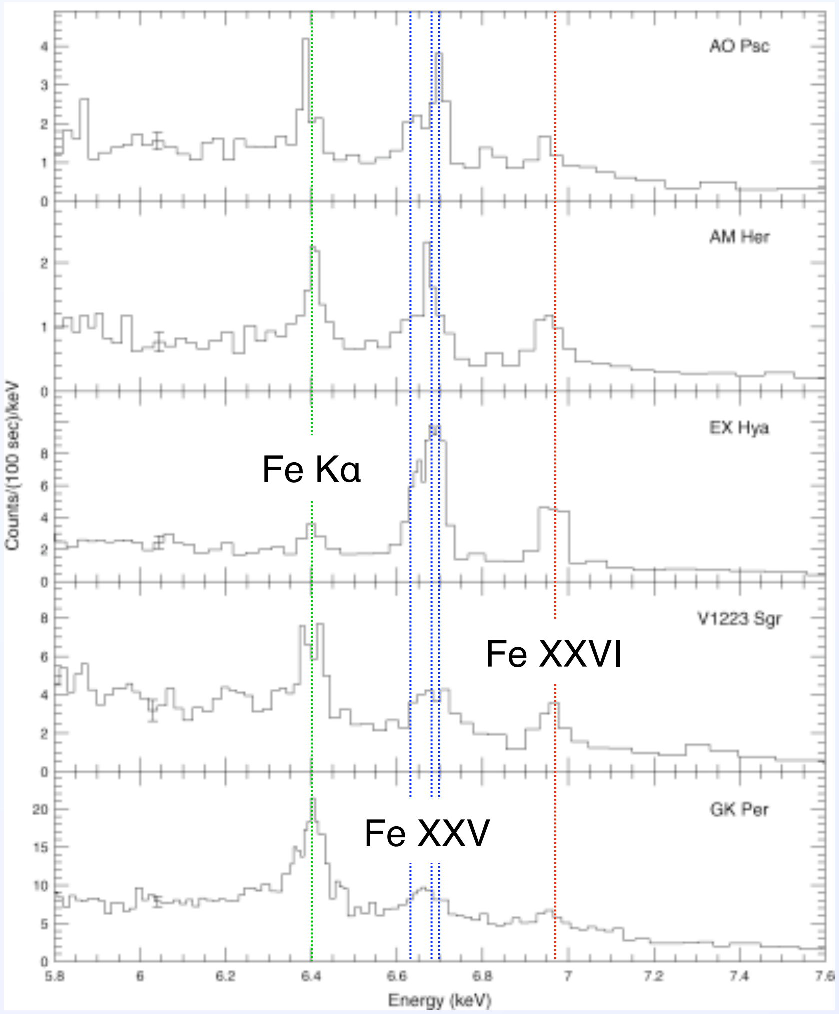

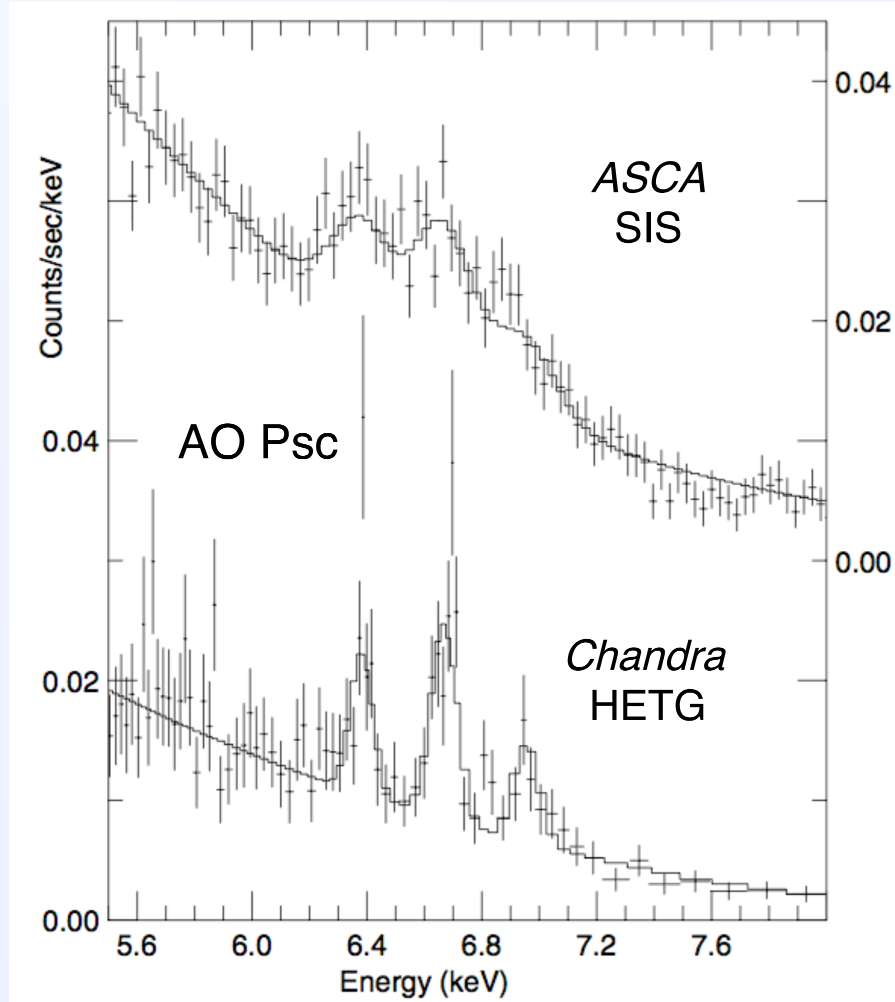

Hellier & Mukai (2004, MNRAS, 352, 1037)

ASCA SIS spectrum of EX Hya

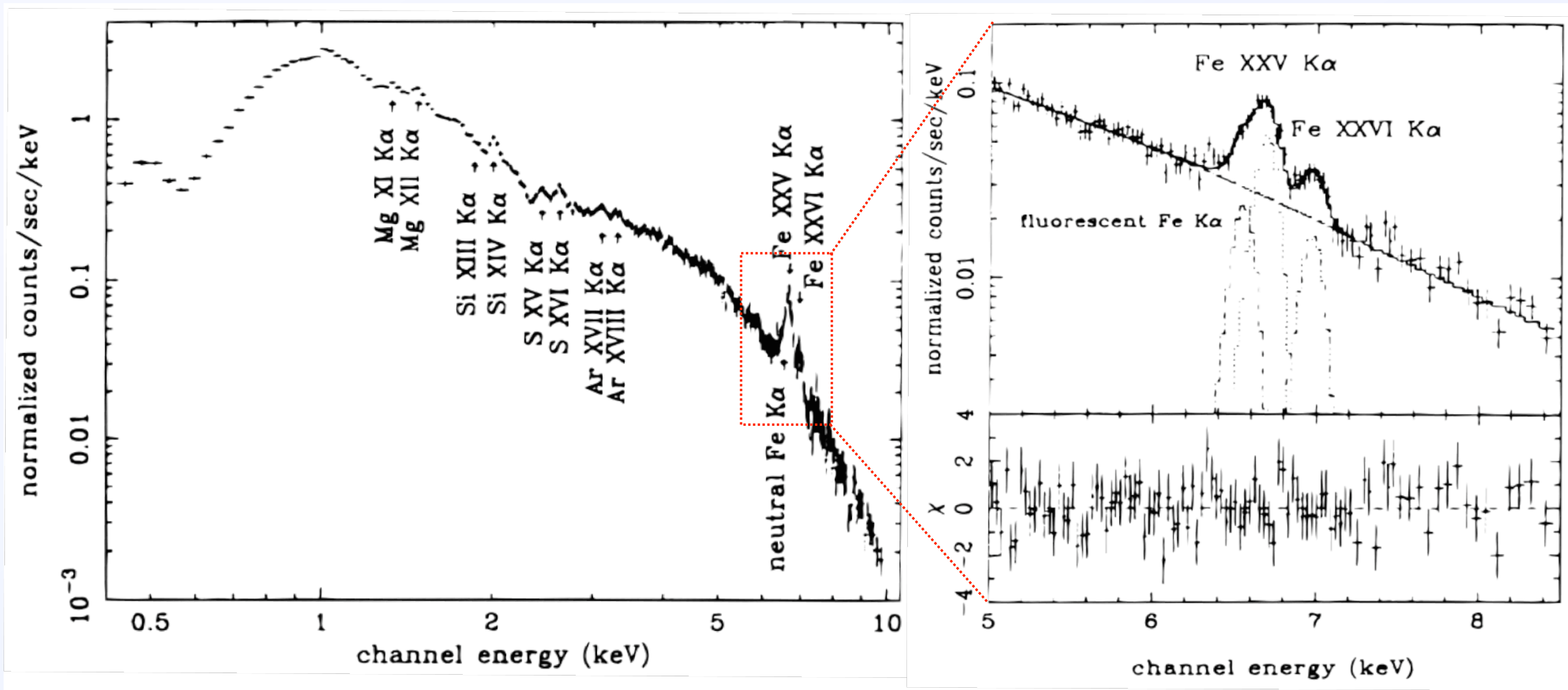

H/He-like line ratios used to measured $kT_{shock} = 15.4^{+5.3}_{-2.6}$ keV hence $M_{wd} = 0.48^{+0.1}_{-0.6}$ $M_\odot$ assuming $kT_{shock} = \frac{3}{8}\mu m_H G M_{wd}/R_{wd}$ and $R_{wd} = 7.8E8\ [(M_{wd}/1.44M_\odot)^{-2/3} - (M_{wd}/1.44M_\odot)^{2/3}]^{1/2}$ cm.

Fujimoto & Ishida (1997, ApJ, 474, 774)

ASCA SIS spectrum of EX Hya, continued

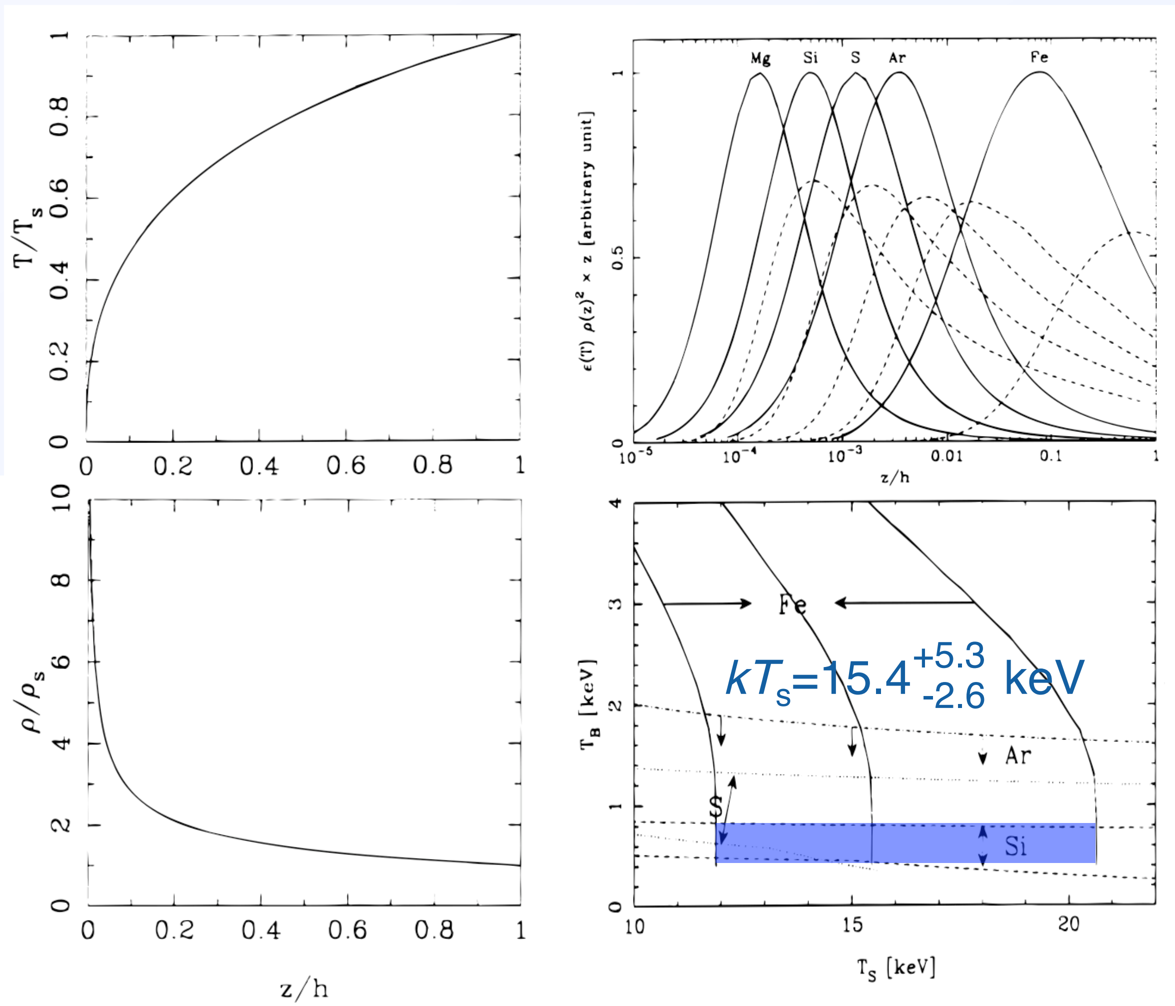

Perfect gas law:

$kT_2 = 3\mu m_H v_2^2$

Strong shock:

$v_2 = v_1/4,\ \rho_2 = 4\rho_1$

Free-fall from infinity:

$v_1 = (2GM_{wd}/R_{wd})^{1/2}$

$kT_s = \frac{3}{8}\mu m_H GM_{wd}/R_{wd}$

$h \ll R_{wd}$

$T_{ion} = T_e$

optically thin

thermal brems cooling

Constant pressure:

$T/T_s \approx (z/h)^{2/5}$

➔ $M_{wd} = 0.48^{+0.10}_{-0.06} M_\odot$

Aizu (1973); Fujimoto & Ishida (1997, ApJ, 474, 774)

EUVE SW 180 ks spectrum of EX Hya

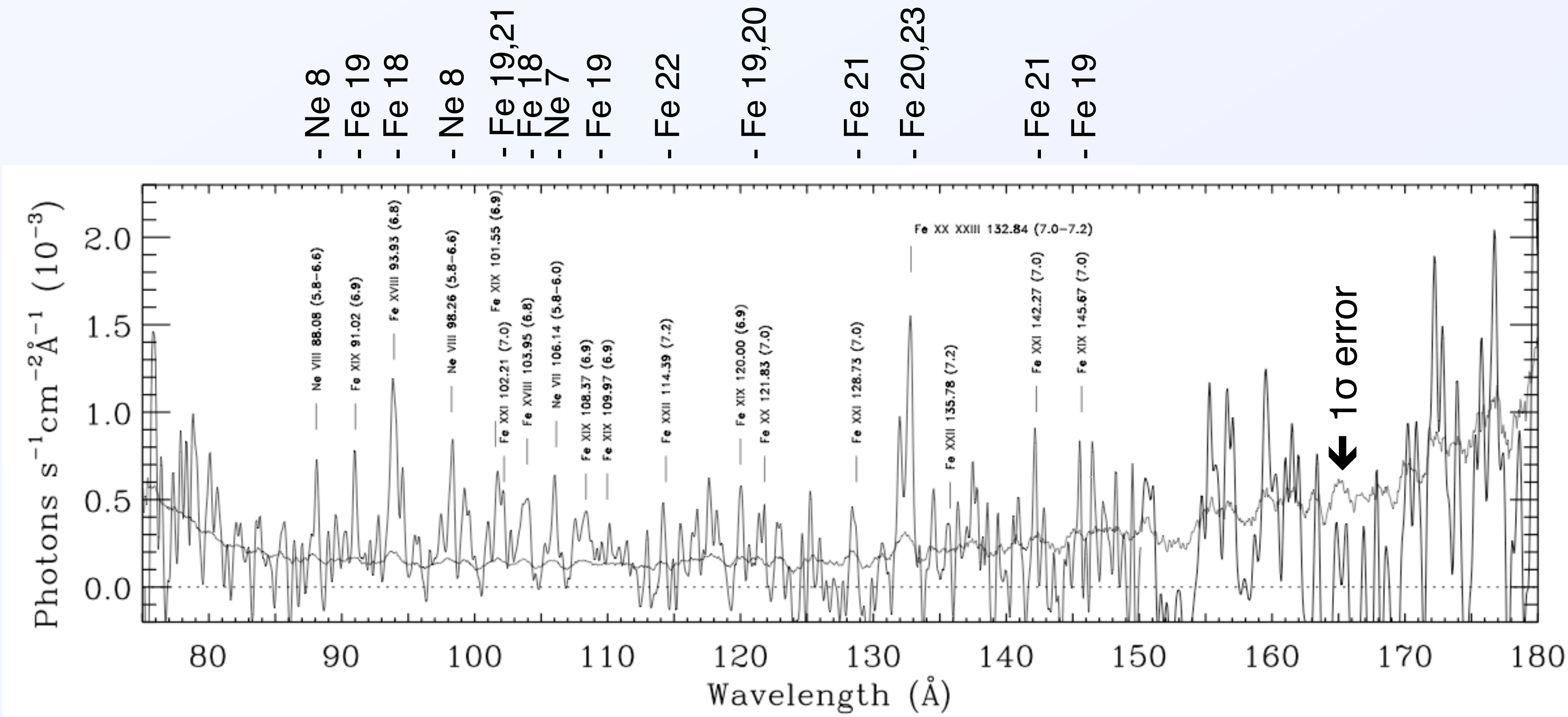

Lines from Ne VII–VIII and Fe XVIII–XXIII ➔ $T \sim 10^{6-7}$ K.

Emission measure and volume ➔ $n_e > 10^{13-15}$ cm^{-3}.

Hurwitz et al. (1997, ApJ, 477, 390)

Chandra HETG 500 ks spectrum of EX Hya

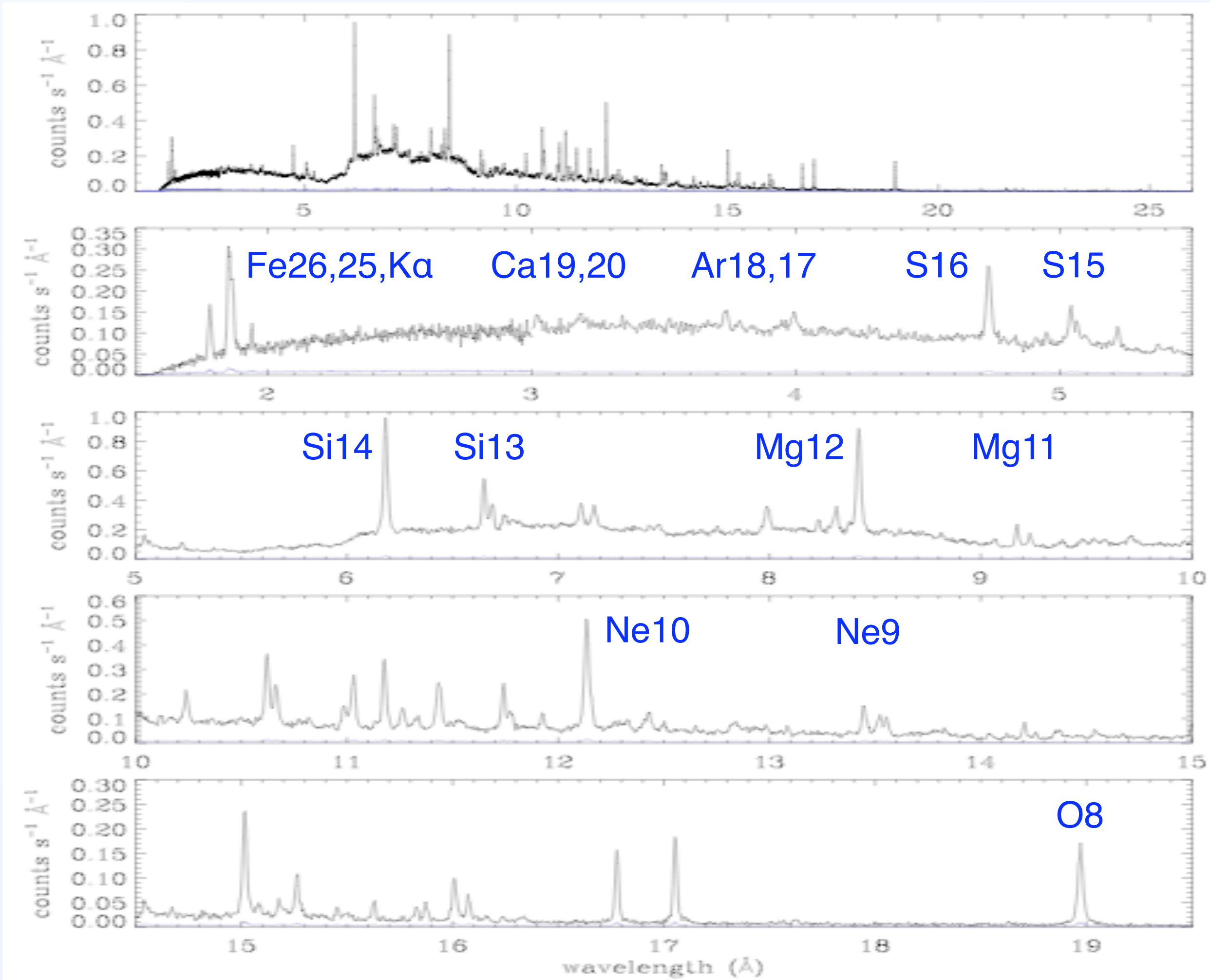

Brickhouse et al. (2006, BAAS, 38, 346)

Comparison of EX Hya (blue) and HR 1099 (red)

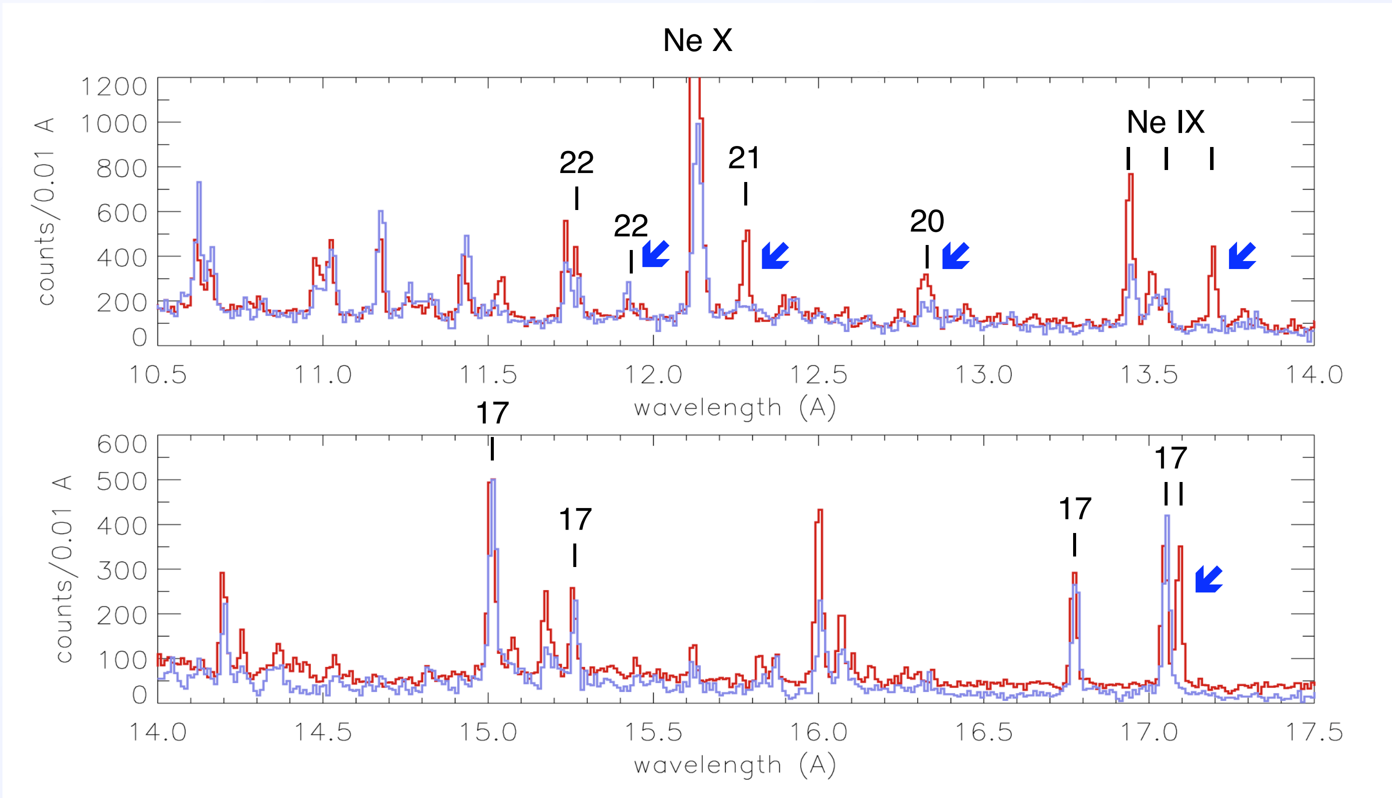

EX Hya is missing lines of Fe XVII λ17.10, Fe XX λ12.80, Fe XXI λ12.26, and has an inverted Fe XXII λ11.92/λ11.77 ratio.

Mauche, Liedahl, & Fournier (2005, in X-ray Diagnostics of Astrophysical Plasmas: Theory, Experiment, & Observation)

The He-like forbidden (*f*) lines are missing in EX Hya

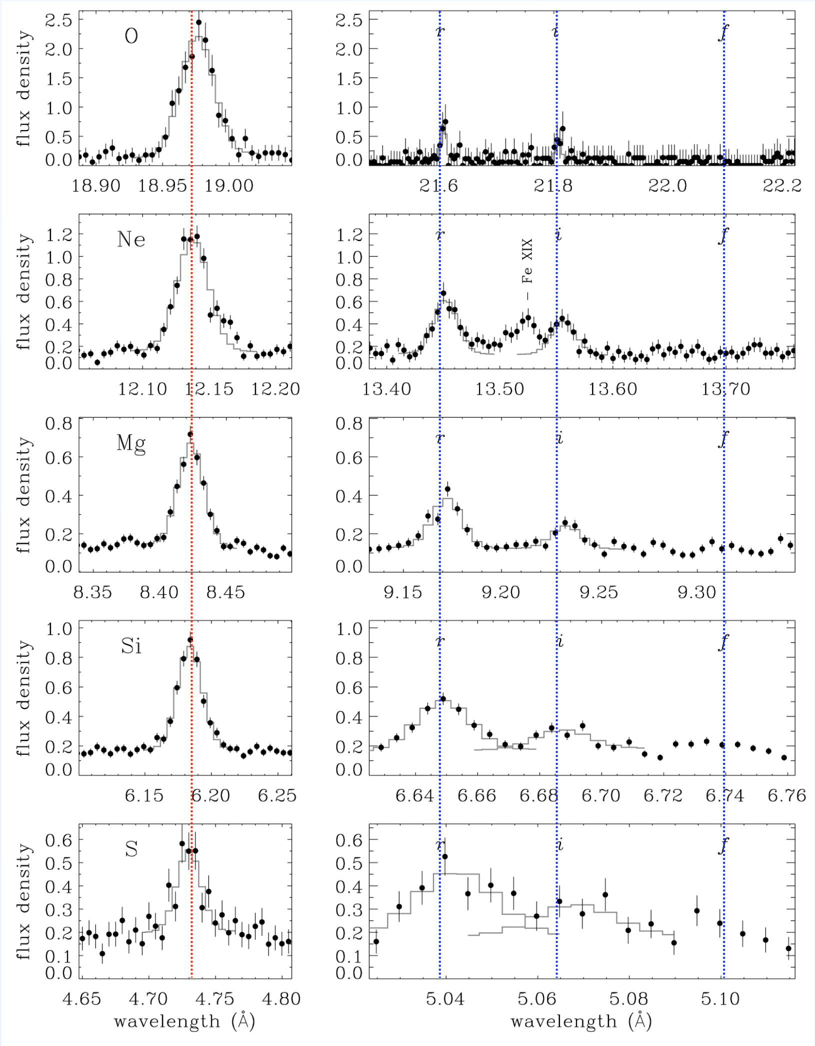

Mauche (2002, in Physics of CVs and Related Objects)

He-like $R = z/(x+y) = f/i$ line ratios in EX Hya

$T_{bb} = 0$ K $\qquad$ $T_{bb} = 30$ kK

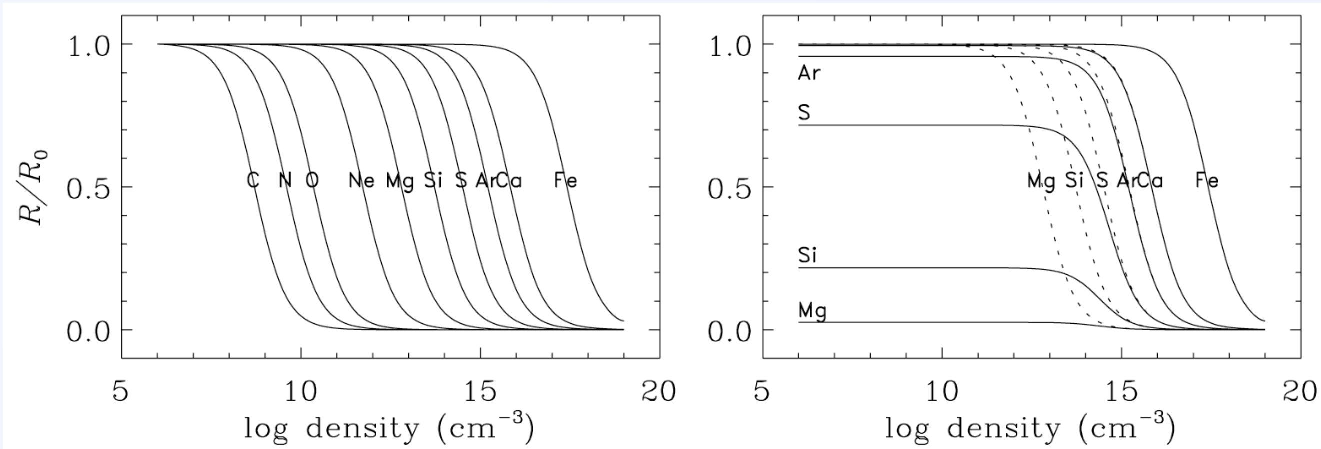

Absence of He-like forbidden lines in EX Hya is plausibly due to photoexcitation.

Mauche (2002, in Physics of CVs and Related Objects)

Theoretical Fe L-shell spectra

Theoretical Fe L-shell spectra were calculated with the Livermore X-ray Spectral Synthesizer (LXSS), a suite of IDL codes that calculates spectral models as a function of temperature and electron density using primarily HULLAC atomic data.

Ion	Levels	Radrate	Colrate
Fe XXIV	76	4,100	1,704
Fe XXIII	116	8,798	6,478
Fe XXII	228	37,300	24,084
Fe XXI	591	227,743	153,953
Fe XX	609	257,765	165,350
Fe XIX	605	240,948	164,496
Fe XVIII	456	141,229	93,583
Fe XVII	281	49,882	33,887

Mauche, Liedahl, & Fournier (2005, in X-ray Diagnostics of Astrophysical Plasmas: Theory, Experiment, & Observation)

Fe XVII

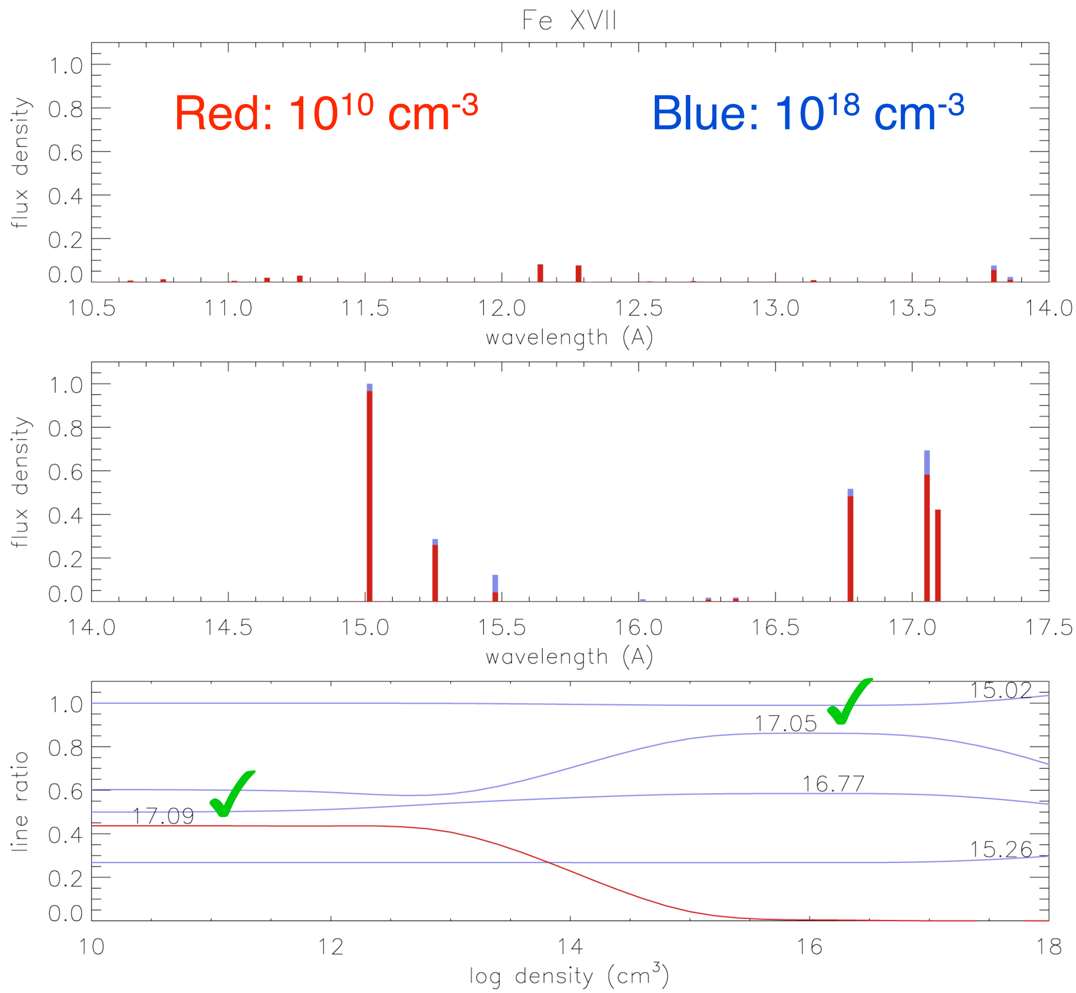

Mauche, Liedahl, & Fournier (2005)

Fe XVIII

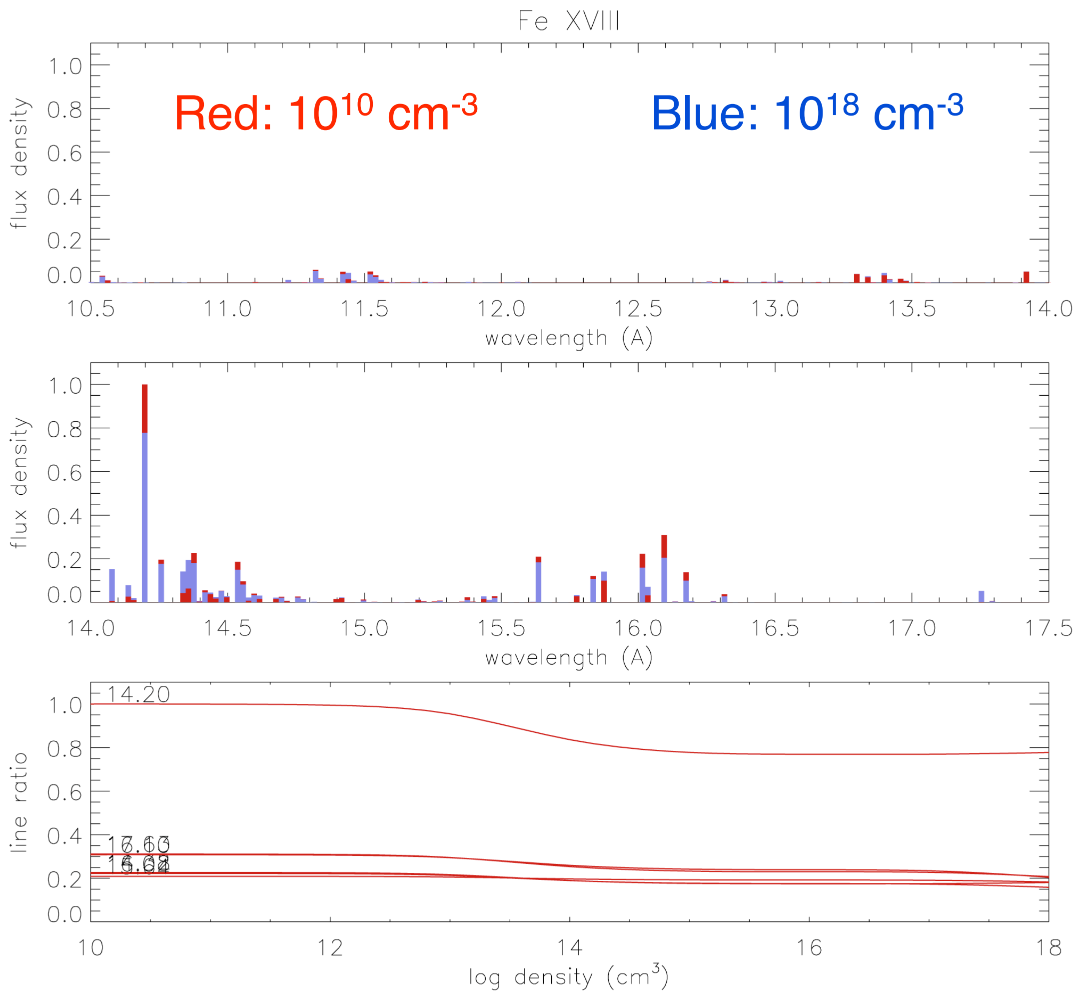

Mauche, Liedahl, & Fournier (2005)

Fe XIX

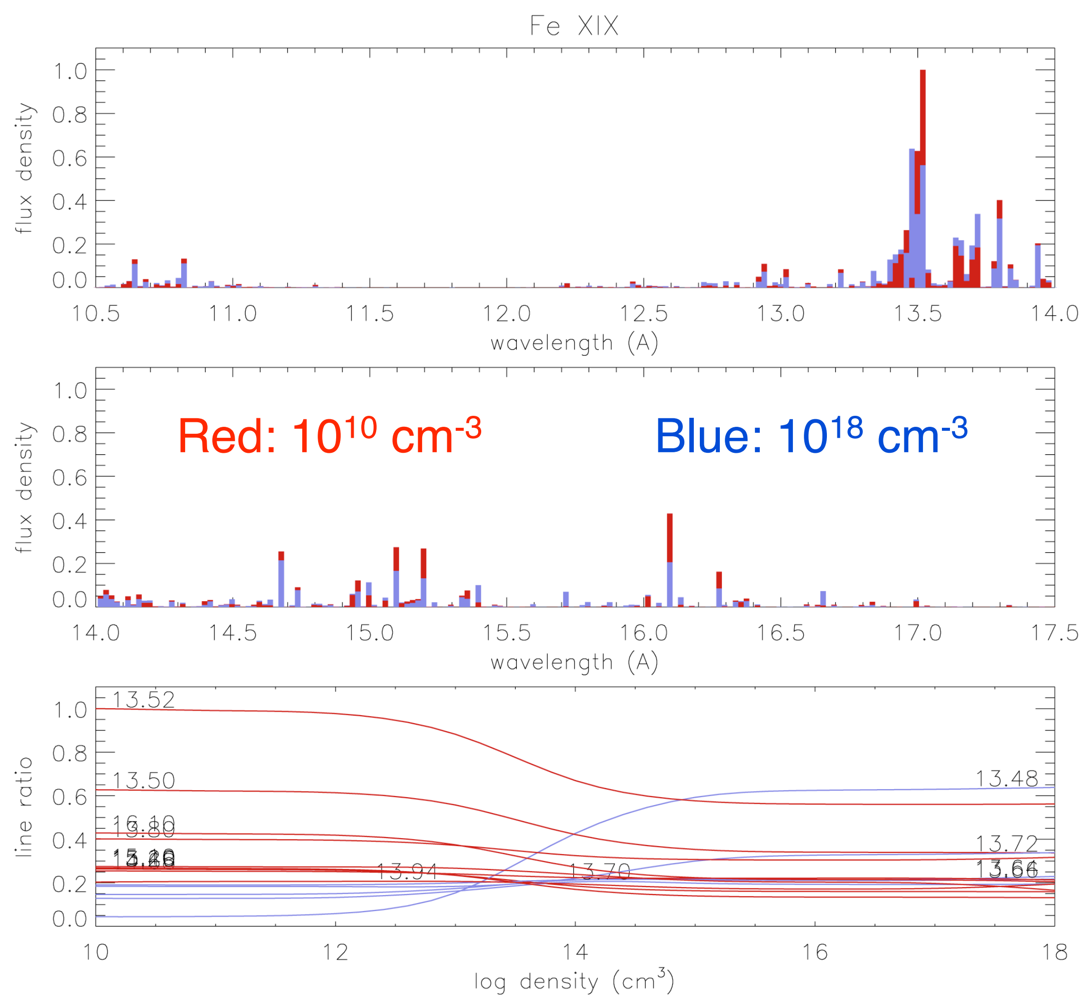

Mauche, Liedahl, & Fournier (2005)

Fe XX

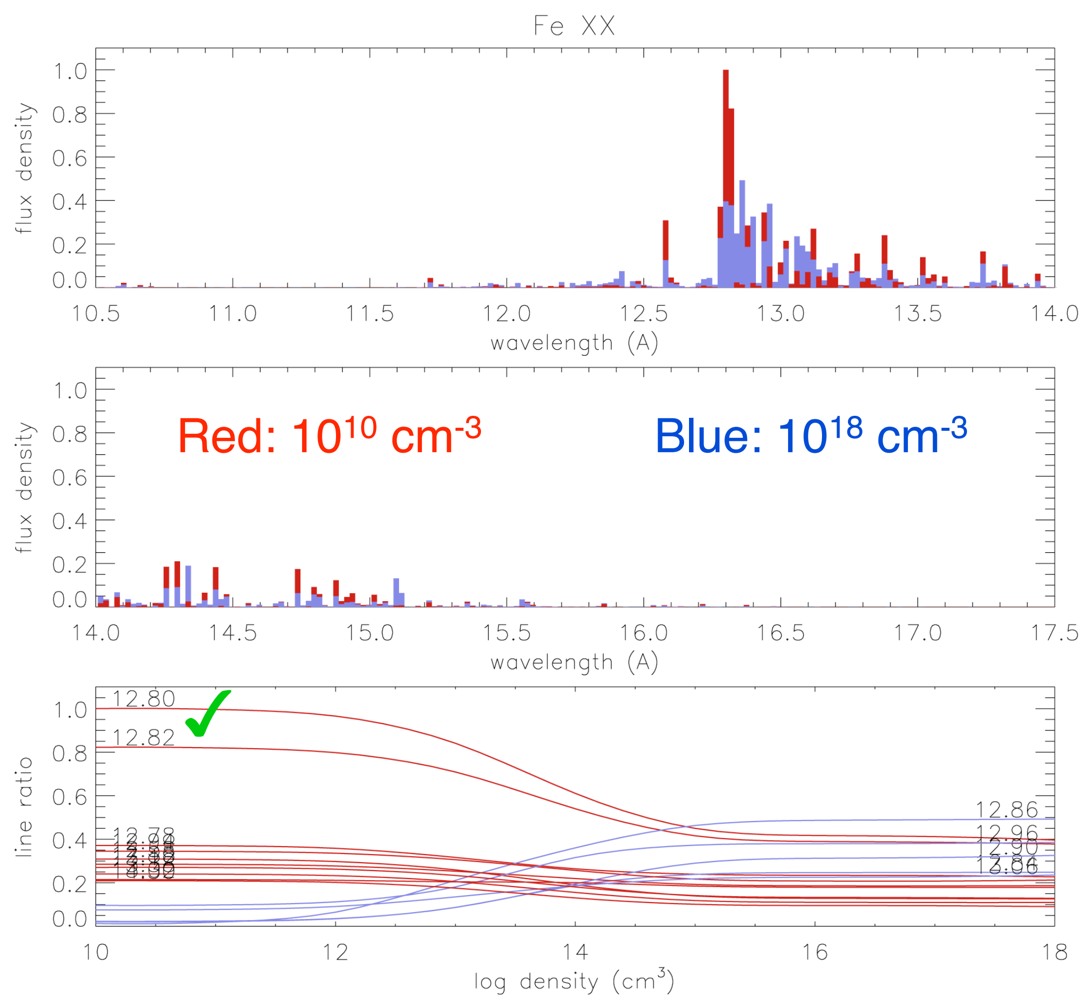

Mauche, Liedahl, & Fournier (2005)

Fe XXI

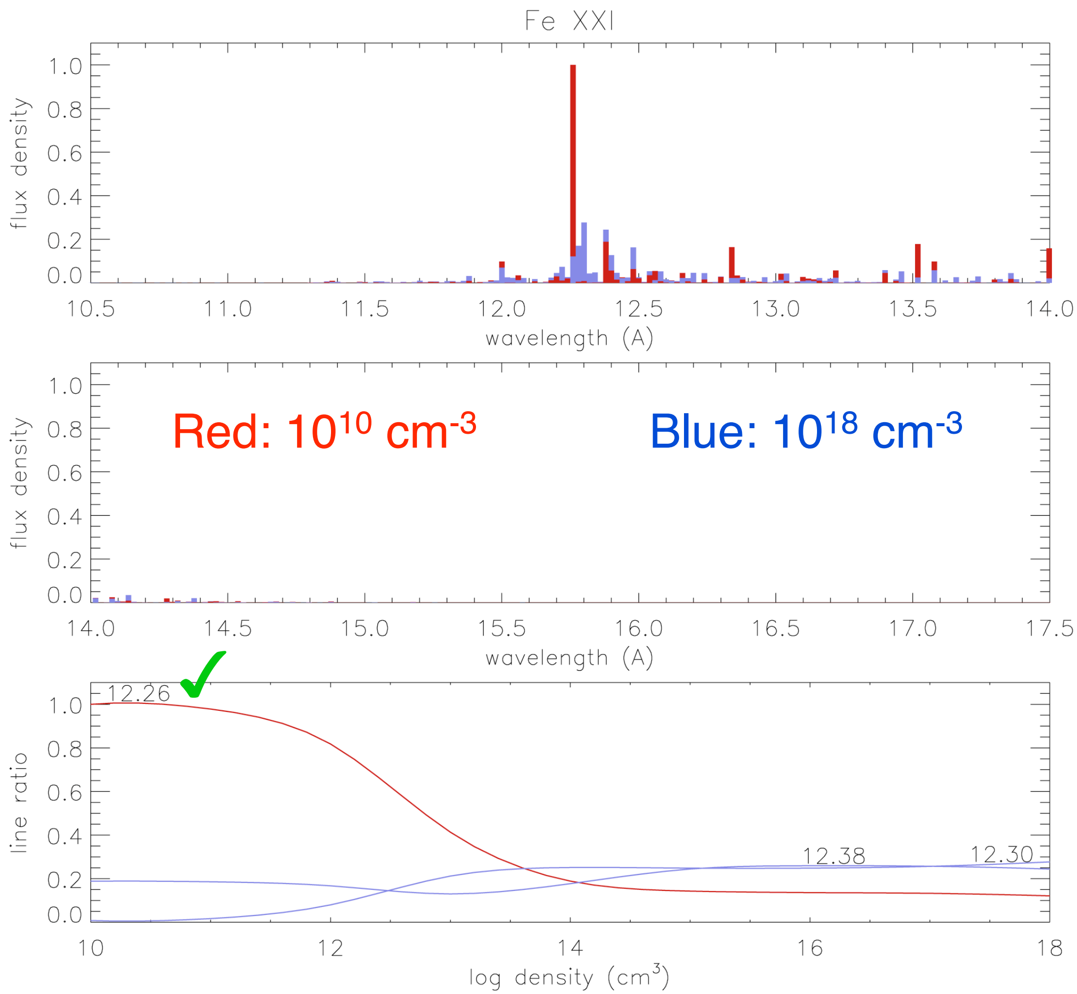

Mauche, Liedahl, & Fournier (2005)

Fe XXII

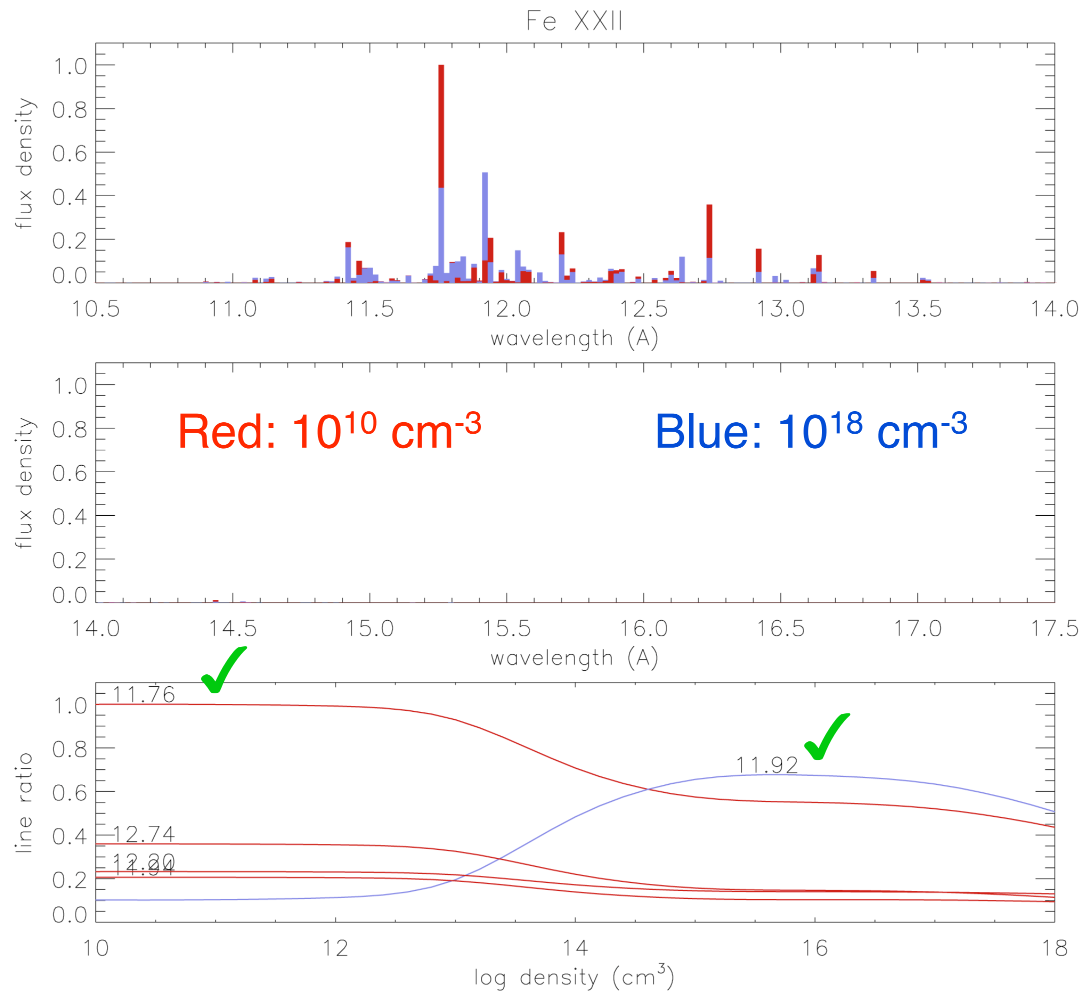

Mauche, Liedahl, & Fournier (2005)

Fe XXIII

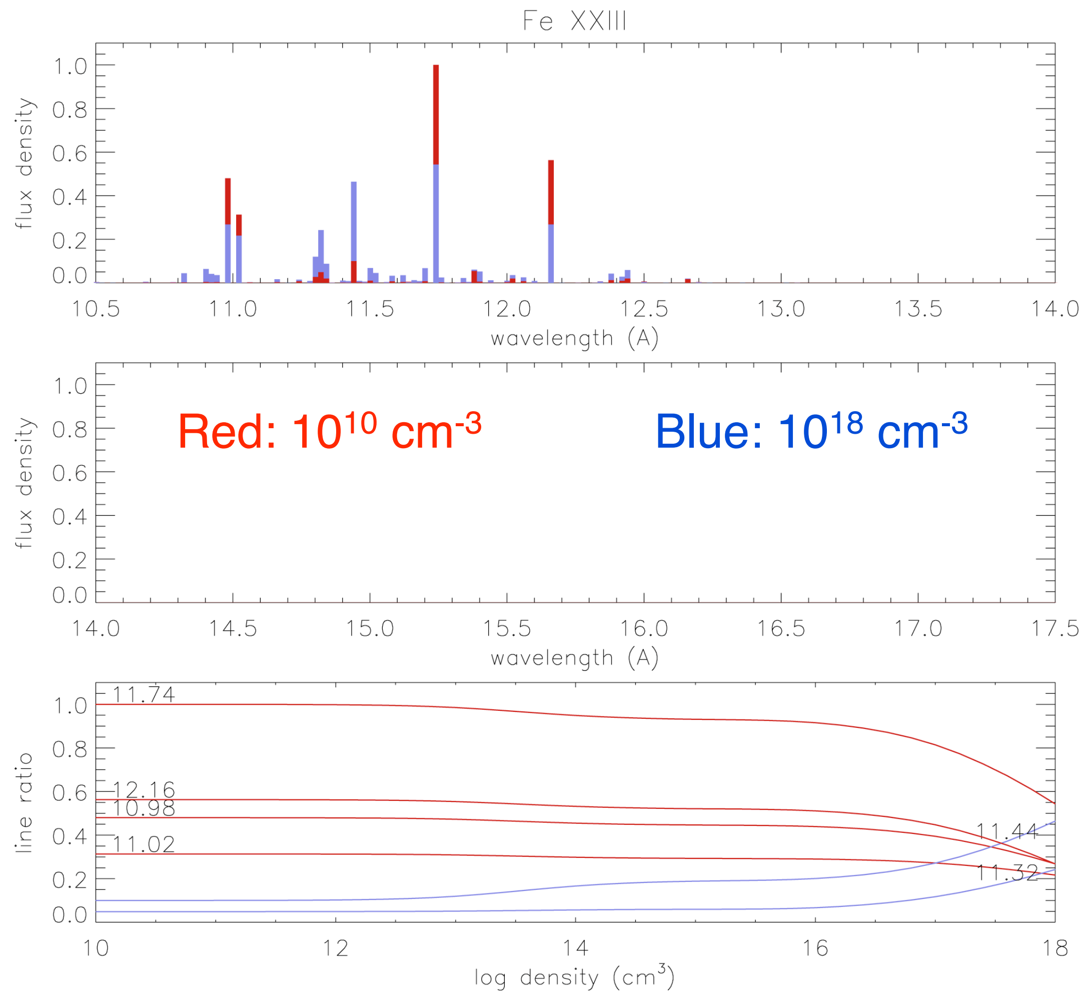

Mauche, Liedahl, & Fournier (2005)

Fe XXIV

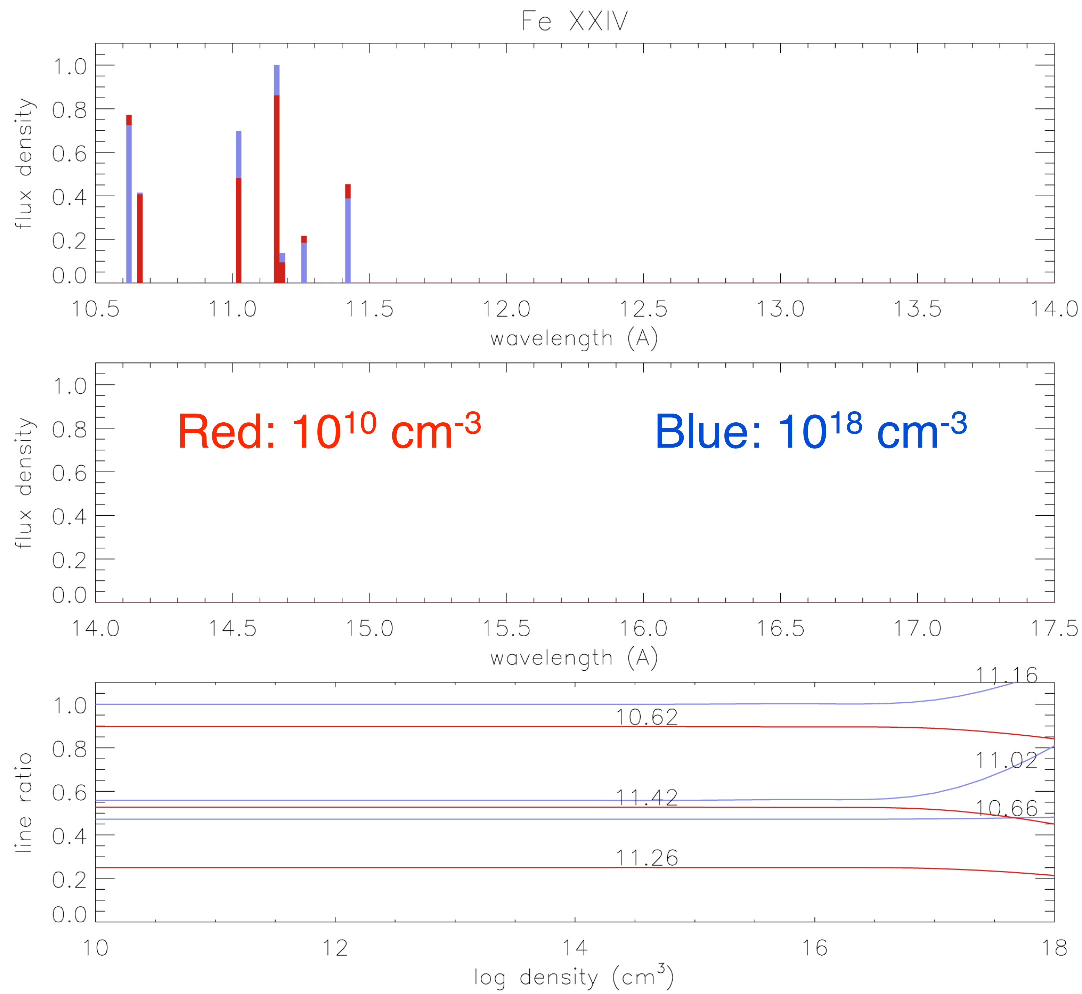

Mauche, Liedahl, & Fournier (2005)

Grotrian diagrams for Fe XVII and Fe XXII

Fe XVII

Fe XXII

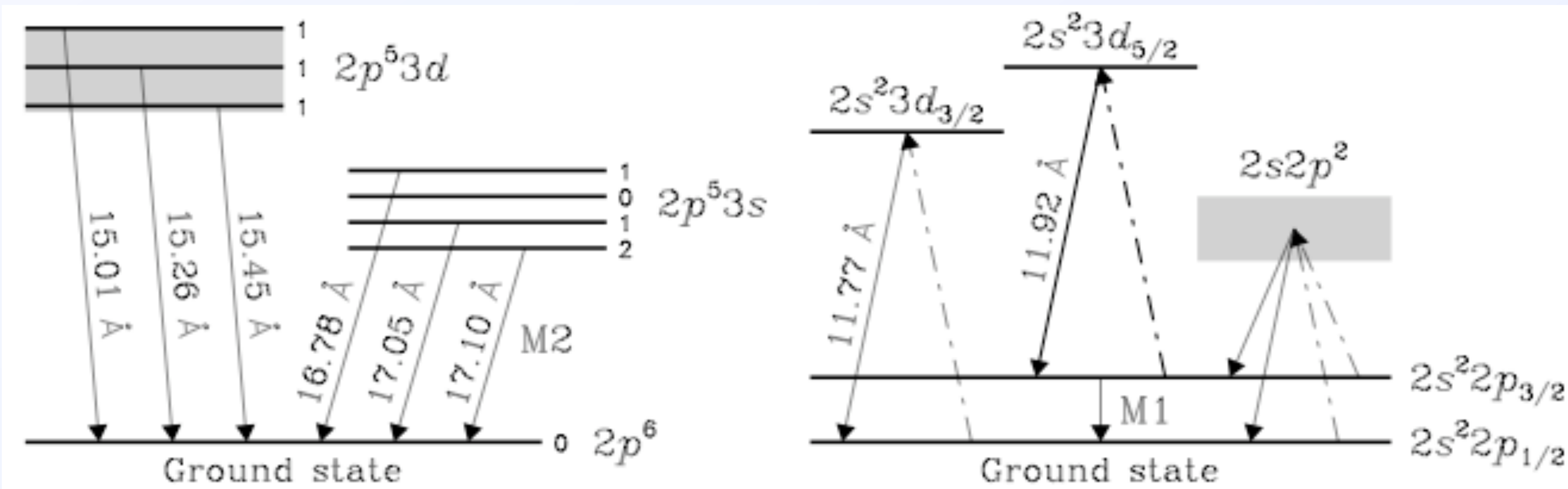

Mauche, Liedahl, & Fournier (2005, in X-ray Diagnostics of Astrophysical Plasmas: Theory, Experiment, & Observation)

Density constraints for EX Hya from Fe XVII λ 17.10/ λ 17.05 and Fe XXII λ 11.92/ λ 11.77

Fe XVII: $n_e > 2\times10^{14}$ cm^{-3}

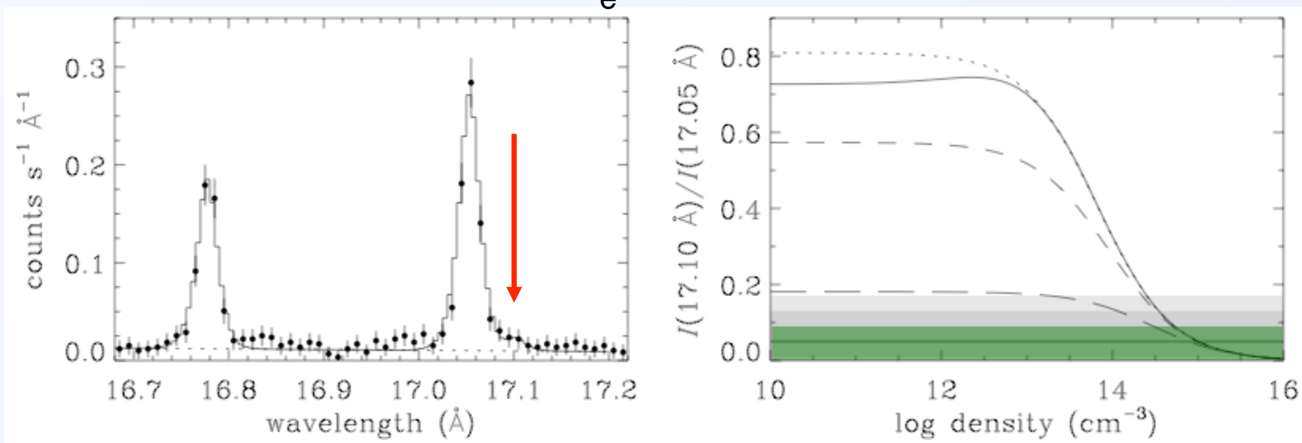

Fe XXII: $n_e \sim 1\times10^{14}$ cm^{-3}

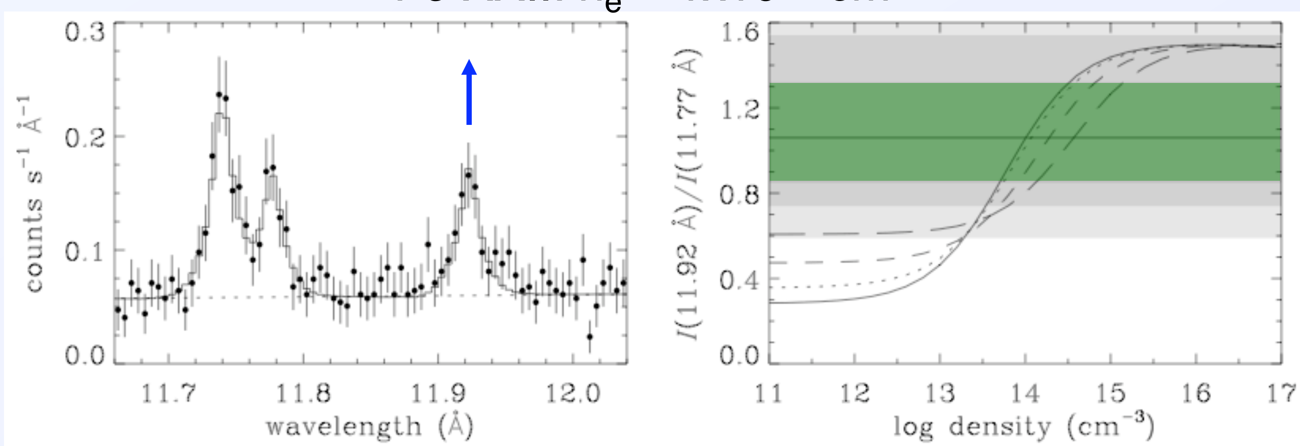

Mauche, Liedahl, & Fournier (2001, ApJ, 560, 992; 2003, ApJ, 588, L101)

Radial velocity variations of the X-ray emission lines of EX Hya

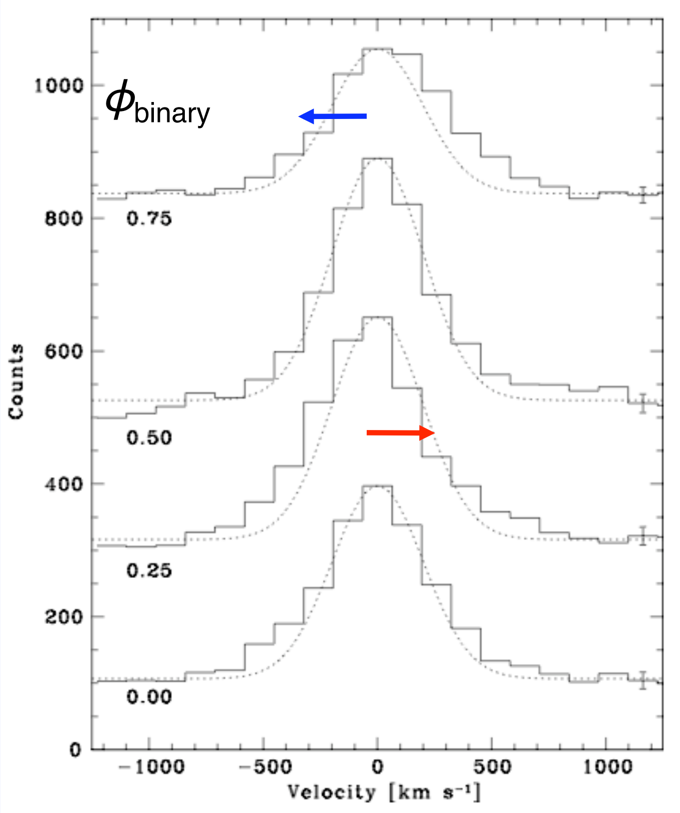

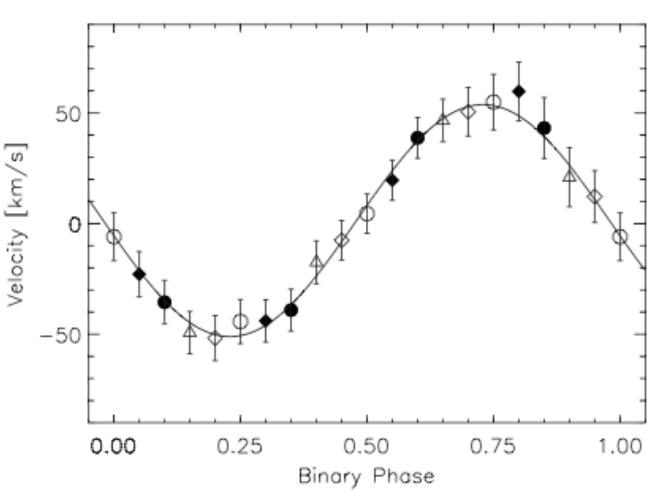

γ = 1.3 +/- 2.3 km s^{-1}
K_{wd} = 58.2 +/- 3.7 km s^{-1}
M_{wd} = 0.49 +/- 0.13 $M_{\odot}$

Dynamically-derived M_{wd} agrees with the value obtained from the Fe XXV/XXVI line ratio in the *ASCA* SIS spectrum of EX Hya (Fujimoto & Ishida 1997).

Or does it? Beuermann & Reinsch (2008) have since revised K_{sec} and hence M_{sec}.

Hoogerwerf, Brickhouse, & Mauche (2004, ApJ, 610, 411)

AE Aqr: many things to many people

Patterson (1979): Oblique Rotator

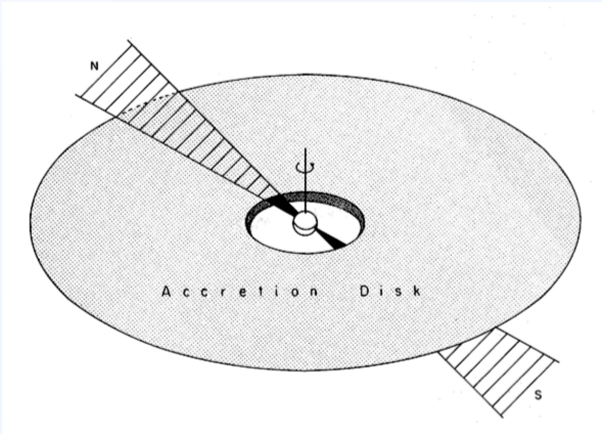

E&H (1996), WHG (1998): Magnetic propeller

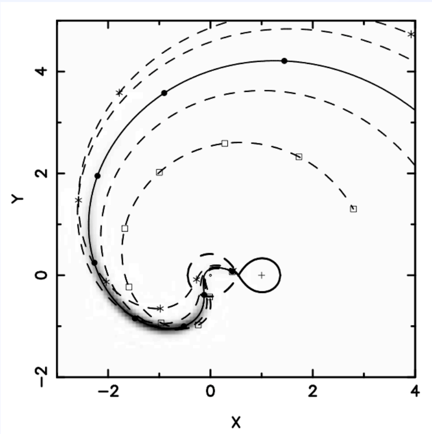

WKH (1997): Diamagnetic Blobs

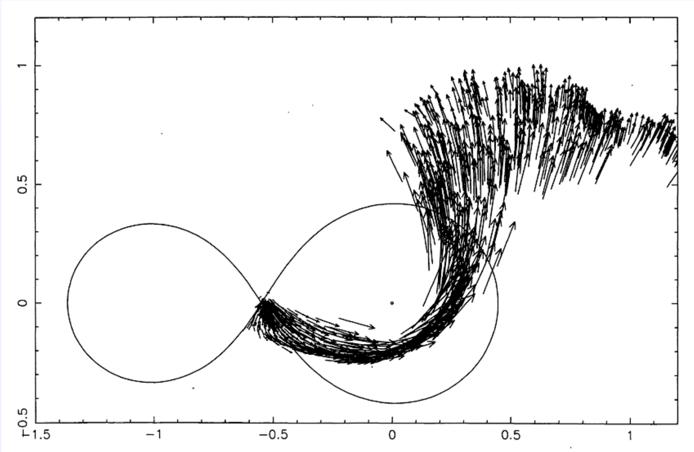

Terada et al. (2008): Cosmic Ray Accelerator

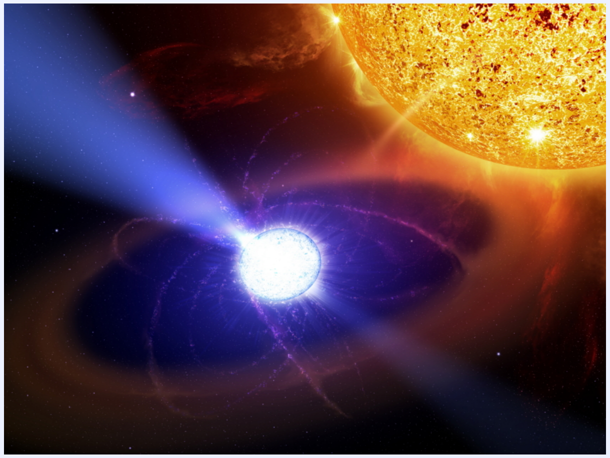

XMM EPIC & RGS spectra of AE Aqr

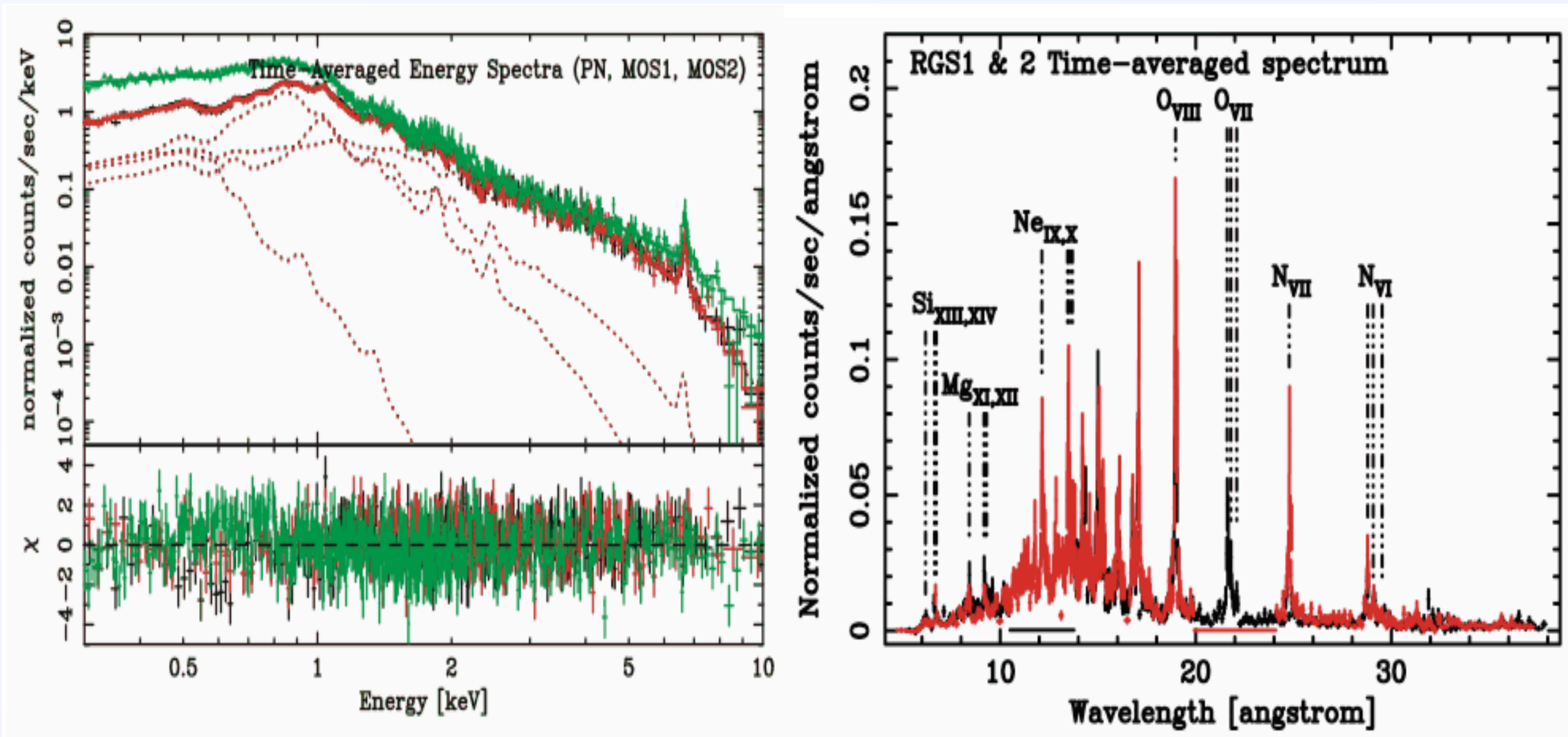

4T VMEKAL fit gives kT = 0.14, 0.59, 1.21, & 4.6 keV, which is cool for an IP.

Itoh et al. (2006, ApJ, 639, 397)

He-like N, O, & Ne density diagnostics derived from the *XMM* RGS spectrum of AE Aqr

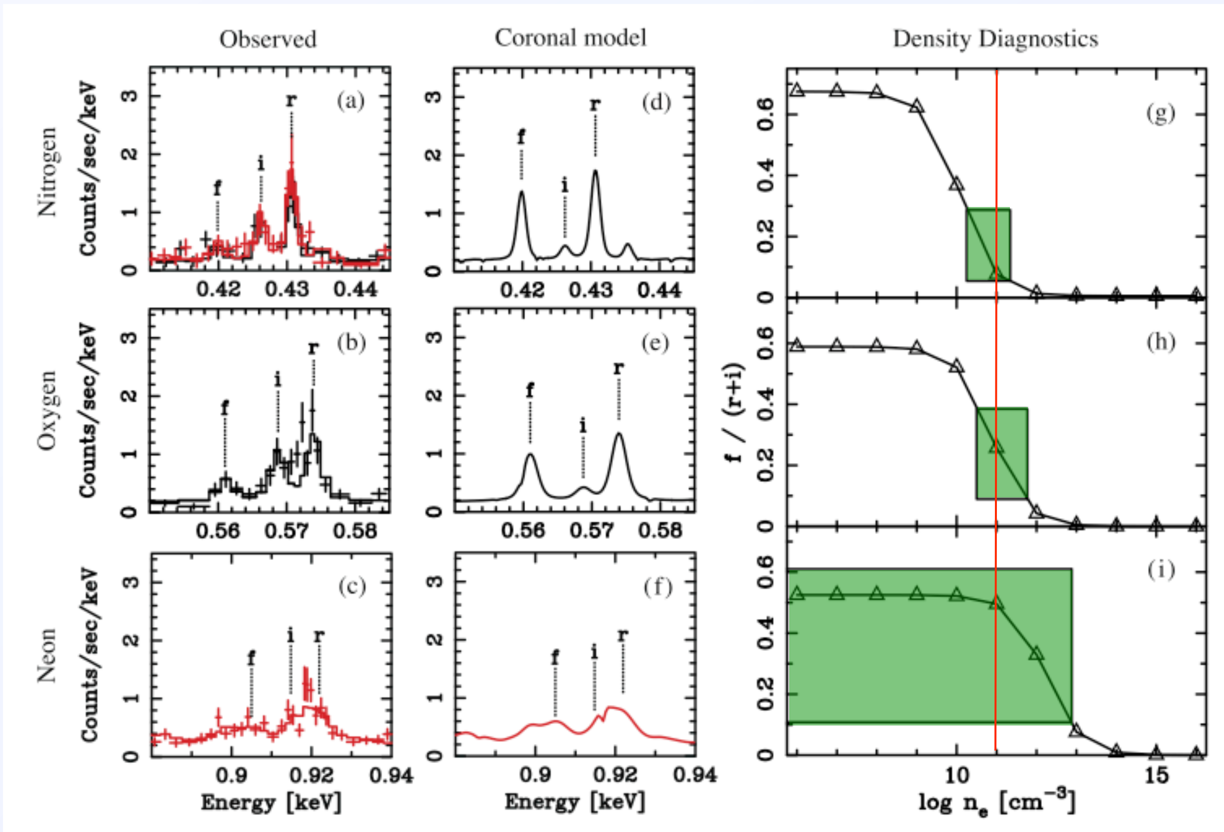

He-like N, O, and Ne *f*/(*r*+*i*) line ratio is consistent with $n_e \sim 10^{11}$ cm^{-3}.

Itoh et al. (2006, ApJ, 639, 397)

2005 multiwavelength observations of AE Aqr

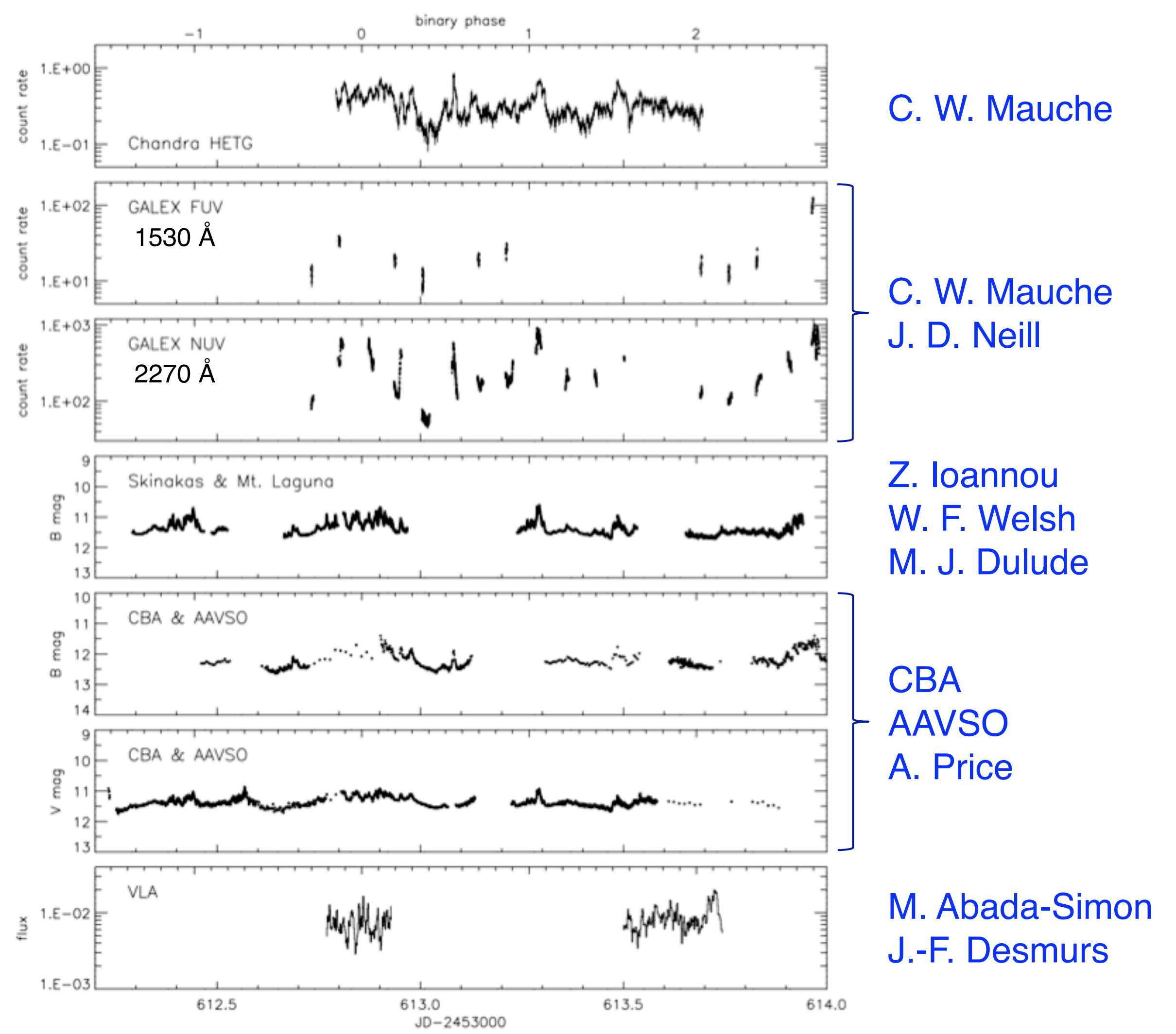

Correlated flares and the 33 s white dwarf spin pulse are observed in the optical through X-ray wavebands.

The radio light curve is uncorrelated with the other wavebands, implying that the radio flux is due to independent processes.

Chandra HETG spin pulse

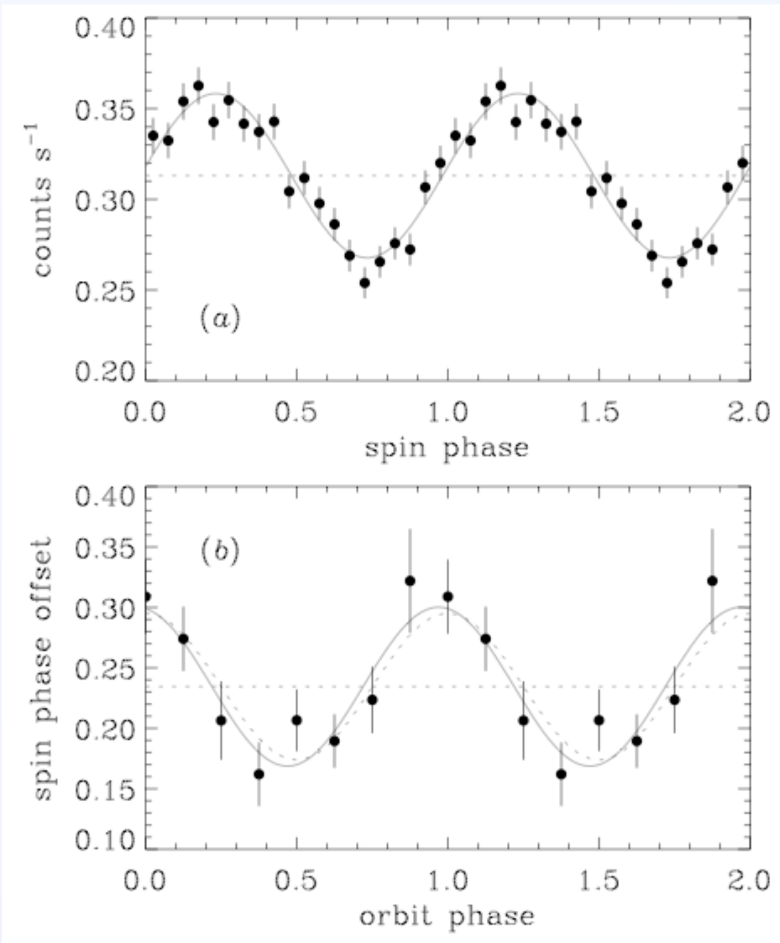

Phase offset of 0.232 ± 0.011 cycles relative to the de Jager et al. (1994) spin ephemeris.

➔ White dwarf is spinning down at a rate that is slightly less than that predicted by the de Jager et al. (1994) quadratic ephemeris.

Spin phase offset variations correspond to a pulse time delay of $a \sin i = 2.17 \pm 0.48$ s.*

➔ X-ray source follows the motion of the white dwarf around the binary center of mass.

*A similar result was derived by de Jager (1995).

Mauche (2006, MNRAS, 369, 1983)

Chandra HETG spectrum of AE Aqr

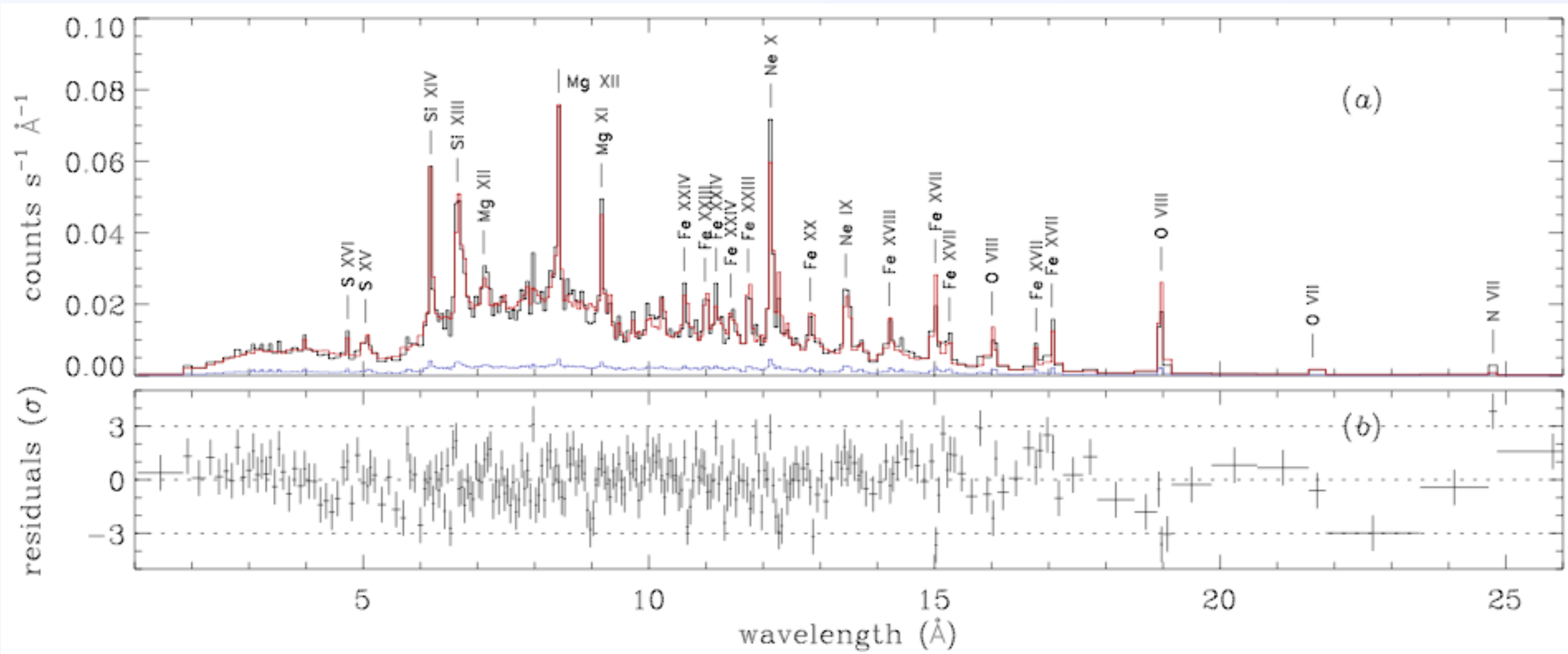

Spectrum is reasonably well fit by a Gaussian emission measure distribution with a peak at log T(K) = 7.16, a width $\sigma = 0.48$, Fe/Fe$_\odot$ = 0.44, other metals $Z/Z_\odot = 0.76$, $EM = 8\times10^{53}$ cm^{-3}, and $L_x = 1\times10^{31}$ $(d/100 \text{ pc})^2$ erg s^{-1}.

Mauche (2009, ApJ, 706, 130)

Chandra HETG He-like triplet *f*/(*i*+*r*) line ratios

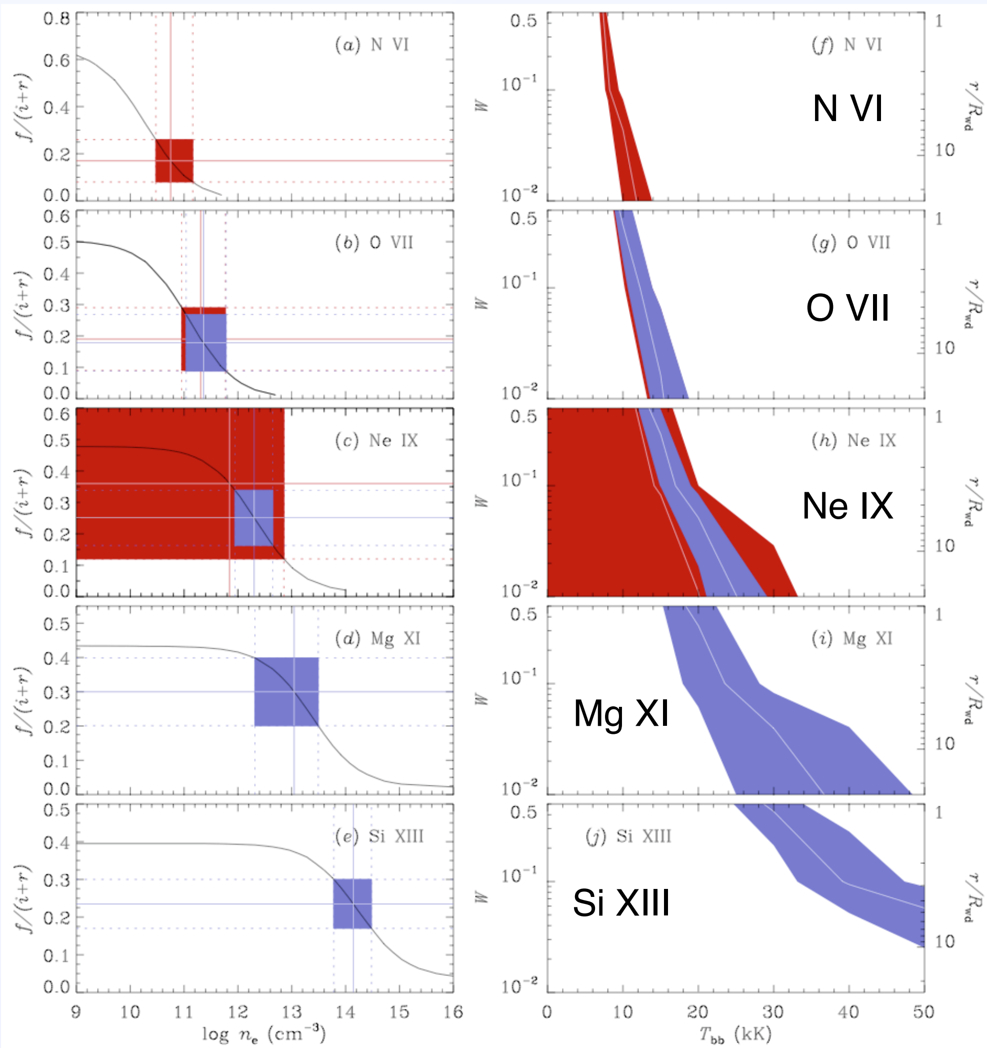

Mauche (2009, ApJ, 706, 130)

Red: *XMM-Newton* RGS*
Blue: *Chandra* HETG

Left: Density increases with temperature from $n_e \sim 6\mathrm{x}10^{10}$ cm^{-3} for N VI to $n_e \sim 1\mathrm{x}10^{14}$ cm^{-3} for Si XIII.

Right: Photoexcitation can mimic high densities, but (at least for the high Z elements) high T_{bb} and/or large dilution factors are required to explain the observed ratios.

➔X-ray plasma is of high density and/or in close proximity to the white dwarf.

*Itoh et al. (2006, ApJ, 639, 397)

Chandra HETG emission line radial velocities

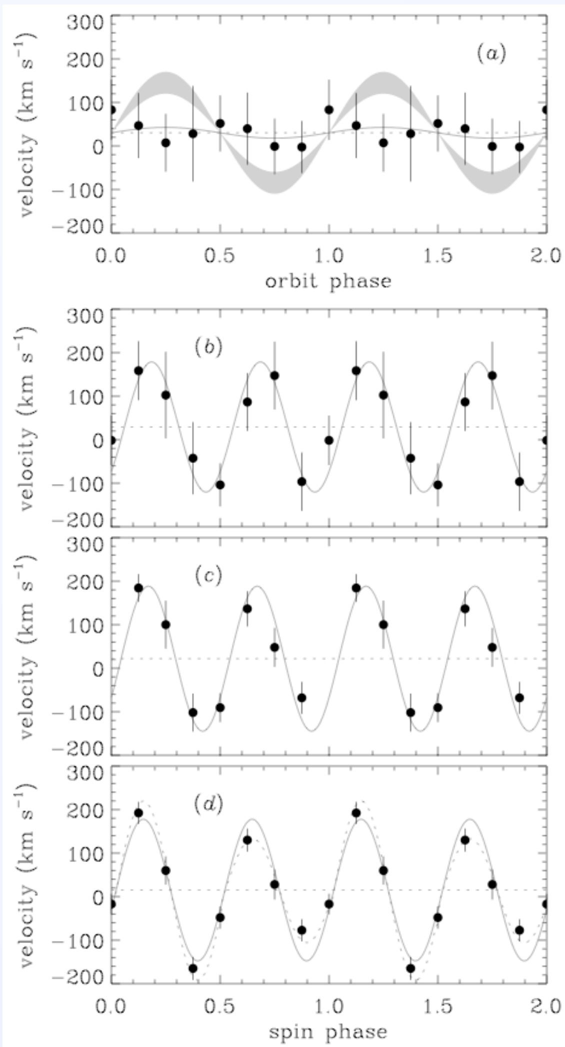

Radial velocities don't appear to vary on the white dwarf orbit phase!

(*a*) composite line profile technique

➔ This is an unexpected result, but differs from the predicted radial velocity of the white dwarf (gray shading) by only 2.3σ.

Radial velocities vary on the white dwarf 33 s spin phase, with two oscillations per cycle.

(*b*) composite line profile technique
(c) cross-correlation technique
(d) boot-strapped cross-correlation technique

➔ X-ray plasma is trapped on, and rotates with, the white dwarf's dipolar magnetic field.

Mauche (2009, ApJ, 706, 130)

Summary of *Chandra* HETG observation of AE Aqr

- The (pulsating component of the) source of X-rays in AE Aqr follows the motion of the white dwarf around the binary center of mass.
- Contrary to the conclusions of Itoh et al. (2006), the majority of the plasma in AE Aqr has a density $n_e > 10^{11}$ cm^{-3}, hence its spatial extent is orders of magnitude less than their estimate of 5×10^{10} cm.
- The radial velocity of the X-ray emission lines varies on the white dwarf 33 s spin phase, with two oscillations cycle and an amplitude K ≈ 160 km s^{-1}, broadly consistent with plasma tapped, and rotating with, the white dwarf's dipolar magnetic field.
- These results are inconsistent with recent models* of an extended, low-density source of X-rays in AE Aqr, but instead support earlier models in which the dominant source of X-rays is of high density and/or in close proximity to the white dwarf.
- To paraphrase Bill Clinton, "*It's accretion, stupid.*"

*Itoh et al. (2006); Ikshanov (2006); Venter & Meintjes (2007)

Mauche (2009, ApJ, 706, 130)